Title: CX_3CR1 Fate-Mapping In Vivo Distinguishes Cochlear Resident and Recruited Macrophages After Acoustic Trauma

Running Title: Macrophage Heterogeneity in the Injured Cochlea

Authors: Sree Varshini Murali [1#], Andrew R Stothert [2#], Elyssa Pereyra [3#], Lyudmila V Batalkina [2], and Tejbeer Kaur [1,2*]

Affiliations: 1. Department of Otolaryngology and Brain Health Institute, Rutgers University, Robert Wood Johnson Medical School, Piscataway, New Jersey, U.S.A., 08854 (present address).

2. Department of Biomedical Sciences, Creighton University, School of Medicine, Omaha, Nebraska, U.S.A., 68178

3. Department of Biology, Creighton University, Omaha, Nebraska, U.S.A., 68178

# Contributed equally

***Corresponding author's name:** Tejbeer Kaur

Corresponding author's address: 675 Hoes Lane West, Rutgers University, Piscataway, New Jersey, USA, 08854

Corresponding author's telephone number: +1 732 235 7311

Corresponding author's email address: tk755@bhi.rutgers.edu; tk755@rwjms.rutgers.edu

ABSRACT

Cochlear injury activates the resident macrophages (RM) and recruits the blood-circulating monocytes and monocyte-derived macrophages (Mo/Mo-M), but their specific functions in the injured cochlea are unknown. It is well established that the chemokine fractalkine receptor (CX_3CR1), expressed by cochlear macrophages, influences the density of those macrophages and promotes synaptic repair and spiral ganglion neuron survival in the injured cochlea. As CX_3CR1 is expressed on both RM and Mo/Mo-M, it remains unclear if CX_3CR1-expressing RM and Mo/Mo-M are distinct and differentially promote SGN survival after cochlear injury. Here, we demonstrate the use of fate mapping via a tamoxifen-inducible CX_3CR1 mouse model ($CX_3CR1^{YFP-CreERT2/wildtype}$:R26RFP) wherein CX_3CR1-expressing RM and Mo/Mo-M are endogenously labeled with different fluorescent reporters to define the heterogeneity in cochlear macrophages regarding their origin, turnover, spatiotemporal distribution, morphology, and fate following a loud acoustic trauma. After 60 days of tamoxifen injections at 4 weeks of age, long-lived cochlear RM were YFP+ RFP+ with 98.0 ± 1.7% recombinant efficiency, and short-lived blood-circulating CX_3CR1 lineage (Mo/Mo-M) were YFP+ RFP- with 2.5 ± 1.1% recombinant efficiency. Following an acoustic trauma of 112 dB SPL at 8-16 kHz octave band for 2 hours, morphologically similar RM and Mo/Mo-M were observed in the spiral ganglion, lamina, ligament, and around the sensory epithelium. Quantification of RM and Mo/Mo-M in the spiral lamina and ganglion revealed distinct spatial and temporal distribution patterns. Furthermore, recruited Mo/Mo-M expressed classical monocyte markers such as Ly6C and CCR2. Both RM and Mo/Mo-M were positive for proliferation marker, Ki67, and negative for apoptotic marker, cleaved caspase-3, suggesting that the overall increase in macrophage numbers in the noise-injured cochlea is a contribution of both the proliferation of RM and recruitment of Mo/Mo-M. Probing for blood-clotting protein, fibrinogen, showed its presence in the cochlea after acoustic trauma, suggesting vascular damage that positively and strongly correlated with the time course of recruitment of blood-circulating Mo/Mo-M in the noise-injured cochlea. These data imply that macrophages in the noise-injured cochlea are heterogeneous regarding their ontogeny, distribution, and fate. They offer a robust tool to study the precise roles of resident and recruited macrophages in healthy and pathological ears.

Summary: Using the novel CX_3CR1 fate-mapping model, our data uncover diversity of macrophages with respect to their ontogeny, turnover, spatiotemporal distribution, and fate in the normal and noise-injured cochlea.

Keywords: Cochlea, Macrophage, Monocyte, Monocyte-derived macrophage, Fate-mapping, Noise-induced hearing loss, Spiral ganglion neurons, Fractalkine.

BACKGROUND

The mononuclear phagocyte system represents a subgroup of leukocytes or white blood cells originally described as a population of bone marrow-derived myeloid cells that circulate in the blood and spleen as monocytes and populate tissues as macrophages in the steady state and during inflammation **(Geissmann et al., 2010, van Furth and Cohn, 1968).** Monocytes are innate-immune effector cells that migrate from blood to tissues during injury or infection and can also differentiate into macrophages during inflammation **(Ginhoux and Jung, 2014, Jung, 2018).** Macrophages are tissue-resident phagocytic cells that play a central role in both steady-state tissue homeostasis, repair, and injury. Macrophages are involved in phagocytosis of apoptotic cells, production of growth factors, pro-inflammatory and anti-inflammatory cytokines to promote wound repair during injury, and processing and presenting antigens to T-lymphoid cells **(Ginhoux and Jung, 2014)**. The resident macrophages in adult tissue in the steady state might arise only from yolk sac-embryonic macrophages (brain microglia), from both yolk sac-embryonic macrophages and fetal liver monocytes (Langerhans cells in skin, alveolar macrophages in lung and Kupffer cells in liver) and can also be replenished by adult bone marrow-derived monocytes (heart and gut macrophages) **(Ginhoux and Guilliams, 2016)**. Hence, macrophages are a heterogeneous cell type that respond differently based on the environmental niche, anatomical location, and distinctive origin.

It is well-established that the developing and adult mammalian cochlea contains a population of local or resident macrophages that are distributed in the spiral ganglion, osseous spiral lamina, spiral limbus, spiral ligament, and stria vascularis of the lateral wall **(Dong et al., 2018, Hirose et al., 2005, Hosoya et al., 2023, Liu et al., 2018, O'MalleyNadol and McKenna, 2016, Okano et al., 2008, Shi, 2010)**. Mild to loud noise trauma, aminoglycoside- or cisplatin-induced ototoxicity, infection, or normal aging of the cochlea is associated with

81 robust activation of resident macrophages and an overall increase in the number of macrophages **(Frye et al.,**
82 **2017, Hirose et al., 2005, Kaur et al., 2015, Sung et al., 2024, Yang et al., 2015)** Whether this increase in
83 macrophage numbers in the damaged cochlea is due to local proliferation of resident macrophages (RM) or
84 recruitment of monocytes (Mo) from blood circulation and their differentiation into macrophages (Mo-M) or both,
85 remains ambiguous. We have recently demonstrated that macrophages play a vital protective role in the
86 damaged cochlea by promoting the long-term survival of spiral ganglion neurons (SGN) and repair of damaged
87 ribbon synapses via neuron-immune fractalkine (CX_3CL1-CX_3CR1) signaling between SGNs (which express
88 CX_3CL1 ligand) and macrophages (which express CX_3CR1 receptor) **(Kaur et al., 2019, KaurOhlemiller and**
89 **Warchol, 2018, Kaur et al., 2015, Manickam et al., 2023, Manickam et al., 2024)**. Notably, CX_3CR1 is present
90 on both RM and Mo/Mo-M and is morphologically similar **(Jung et al., 2000)**, making these two macrophage
91 populations indistinguishable by standard immunohistochemical techniques. Thus, it remains unclear whether
92 CX_3CR1-expressing RM or infiltrated Mo/Mo-M are functionally distinct and differentially promote SGN survival
93 in the injured cochlea. To define the mediators of macrophage-induced neuroprotection and to harness the
94 protective capacity of these cells clinically, it is necessary to delineate the specific cell type (i.e., CX_3CR1-
95 expressing RM or Mo/Mo-M) that promotes synaptic repair and SGN survival after cochlear injury.

96 In the current study, we utilized a fate mapping technique by crossing a tamoxifen-inducible Cre mouse line
97 (CX_3CR1YFP−CreER/YFP−CreER) to a red fluorescence protein (RFP) Cre reporter mouse line (R26RFP)
98 **(Goldmann et al., 2013, O'KorenMathew and Saban, 2016b, Parkhurst et al., 2013, Plemel et al., 2020a)**
99 wherein CX_3CR1-expressing RM and Mo/Mo-M are endogenously labeled with different fluorescent reporters to
100 define the heterogeneity in cochlear macrophages regarding their origin, spatiotemporal distribution,
101 morphology, and fate following an acoustic trauma that causes permanent hearing loss. We show here that the
102 progeny of this crossing, CX_3CR1YFP−CreER/wt:R26RFP, can be used to differentially label resident
103 macrophages (RM) versus recruited Mo-derived cells (Mo/Mo-M) in the cochlea. This system works by tamoxifen
104 pulsing mice to temporarily activate Cre in constitutively CX_3CR1-positive (YFP+) cells, i.e., Mo and cochlear
105 resident macrophages. The activated Cre removes a stop codon controlling RFP expression such that YFP+
106 cells become RFP+. Once the tamoxifen is no longer bioavailable, Cre is inactive, and no new YFP+ cells can
107 express RFP. This step is followed by a “wash out” period of several weeks wherein RFP expression is lost in

108 Mo (as they turnover in circulation because of ongoing, lifelong hematopoiesis), whereas expression is naturally
109 and indefinitely retained by cochlear RM (because they are long-lived).

110 Using this fate mapping system, in conjunction with flow cytometry and histology, we demonstrate that
111 macrophages in the noise-injured cochlea are heterogeneous regarding their ontogeny, spatial and temporal
112 distribution, and fate. Furthermore, the overall increase in macrophages in the noise-injured cochlea is due to
113 the contribution of both the proliferation of RM and the recruitment of Mo/Mo-M, the latter is associated with a
114 leaky vasculature. This study offers a robust tool to study the isolated roles of resident and recruited
115 macrophages in healthy and pathological ears and to define their neuroprotective functions in the noise-injured
116 cochlea. These findings are likely relevant in other cochlear disease models with myeloid cell involvement, such
117 as hearing loss due to ototoxic drugs, bacterial and viral infections, synaptopathy, biological aging, genetics, and
118 sudden sensorineural hearing loss, as well as associated comorbidities including diabetes, cardiovascular
119 diseases, depression, dementia, and cognitive decline.

120

121 **MATERIALS AND METHODS**

122 **Mice.** $CX_3CR1YFP-CreER/YFP-CreER$ [stock No. 021160] and the Cre reporter mouse line, Rosa-lsl-tdTomato
123 (R26RFP) [stock No. 007914], were purchased from Jackson Laboratories (Bar Harbor, Maine). Efforts were
124 made to minimize animal suffering and reduce the number of animals used for experiments. The animals were
125 housed in a temperature- and humidity-controlled environment in autoclaved cages in groups of 5 under a 12 h
126 light/12 h dark cycle and fed *ad libitum*. To confirm the genotype of the mice, extracted genomic DNA was
127 subjected to polymerase chain reaction (PCR) using forward and reverse primers described in **Table 1**. All
128 aspects of animal care, procedures, and treatment were conducted according to the National Institute of Health
129 guidelines and approved by the Animal Care and Use Committee of Creighton University and Rutgers University.

130

131 **Tamoxifen or corn oil (vehicle) injection.** Tamoxifen (Sigma-Aldrich) was dissolved in corn oil (Sigma-Aldrich)
132 to a stock concentration of 10 mg/ml. 75 mg/kg of tamoxifen was injected intraperitoneally (i.p.) twice, with one
133 day in between injections. Mice were approximately 4 weeks of age when given tamoxifen.

134

135 **Noise exposure.** For noise exposure, we implemented the methodology described in our previous work
136 **(Manickam et al., 2023)**. Briefly, conscious and freely moving mice were subjected to a 2-hour exposure to
137 octave band noise (8–16 kHz) at a consistent intensity of 112 dB SPL, which imparts permanent hearing loss
138 **(Sautter et al., 2006)**. The exposure was performed within a sound-attenuating chamber (WhisperRoom) lined
139 with acoustic foam. The mice were housed either singly or in pairs within modified compartmentalized cages
140 from which food, water, and bedding materials had been removed. These cages were arranged with a maximum
141 of two units positioned directly beneath an exponential horn attached to a speaker (JBL). The acoustic stimulus
142 was computer-generated via customized LabVIEW software interfaced with an audio card (Lynx E22), producing
143 a filtered pure tone (8-16 kHz) that was subsequently amplified via a power amplifier (Crown Audio) connected
144 to the horn speaker. Each exposure session was preceded by calibration via a quarter-inch condenser
145 microphone (PCB) to verify the target sound pressure level (SPL), which varied by ±1 dB across the
146 compartments in the cage. The control groups consisted of unexposed age-matched mice.
147
148 **Cochlea and Blood harvest.** Mice were deeply anesthetized with lethal doses (250 mg/kg) of pentobarbital
149 sodium (Trade Name-Fatal Plus) or pentobarbital sodium and phenytoin sodium (trade name-Euthasol). Before
150 respiratory arrest, mice were perfused by transcardiac route with phosphate-buffered saline (PBS) (Fisher
151 Scientific, catalog #BP661-10) or 4% paraformaldehyde (PFA) (Fisher Scientific, catalog #50980495) in
152 0.1 M phosphate-buffered (PB) solution. Temporal bones and blood were harvested. Blood was collected via
153 terminal cardiac puncture before perfusion. Withdrawn blood was immediately incubated for 15 min at room
154 temperature in a 0.2% Heparin solution (ScienCell, catalog #0863) to prevent coagulation. Heparinized blood (1
155 ml) was treated with 10 ml of 1× Red Blood Cell Lysis Buffer (Invitrogen, catalog #00-4333-57) for 5 min at room
156 temperature with gentle agitation and subsequently thoroughly washed with PBS, pelleted at 300 × *g* for 5 min,
157 and then resuspended in 1 ml of cell staining buffer (BioLegend, catalog #420201) before cell counting,
158 immunolabeling, and flow cytometry.
159
160 **Flow cytometry.** Single-cell suspensions of lysed blood were incubated for 10 min on ice in a blocking solution
161 containing 2% Fc Block and subsequently stained with a combination of fluorophore-conjugated primary

antibodies against CD45, CD11b, Ly6G, and Live/Dead Fixable Violet Dead Cell Stain. Samples were incubated in the dark and on ice for 30 min. After completion of staining, cells were washed with 1 ml of cell staining buffer (BioLegend, catalog #420201), pelleted at 300 × *g* for 5 min, resuspended in 200 µl of cell staining buffer, and fixed with 4% PFA in PBS. Data were acquired with the YETI Cell Analyzer (Propel Labs) using Everest Software (Bio-Rad Laboratories). Gating strategy and raw flow cytometry data were analyzed using FlowJo software (TreeStar). Cell gating was initially set using forward-scatter versus side-scatter plots of all events that corresponded to the size of cells. These cells were gated and labeled "blood cells." These cells were then gated using the Live/Dead stain, gating for live cells only. Live cells were then gated for singlets (single-cell events) by comparing forward-scatter width and side-scatter area. Singlets were then analyzed for the presence of leukocytes using CD45 expression. CD45+ cells were then further analyzed for myeloid lineage using CD11b. Granulocytes were excluded by gating for CD45+ CD11b+ Ly6G+ cells. Finally, CD45+CD11b+Ly6G- myeloid cells in blood were analyzed for the percentage of RFP+ and RFP- expression at various days after tamoxifen injections. **Table 2** describes all antibodies and probes used in the study.

Immunohistochemistry. Cochlear microdissected whole mounts or frozen mid-modiolar cross sections (20-25 µm) were rinsed with PBS (Fisher Scientific, catalog #BP661-10) at least 3 times for 15 minutes each time and incubated at room temperature for 2 h in blocking solution containing 5% normal horse serum (Sigma-Aldrich, catalog #H0146) in 0.2% Triton X-100 (Sigma-Aldrich, catalog #A16046AP) in PBS. Tissue was incubated overnight at room temperature with the following primary antibodies: anti-CD45, anti-GFP/YFP (to enhance visualization of CX_3CR1YFP-expressing macrophages), anti-cleaved caspase-3, anti-Ki67, anti-fibrinogen, anti-Ly6C, and anti-CCR2. Following incubation in primary antibodies, specimens were rinsed for 15 minutes in PBS, repeated 3 times, and treated for 2 h at room temperature in species-specific secondary antibodies conjugated to either DyLight-405 or -647 (1:500, Jackson ImmunoResearch Laboratories) or AlexaFluor-488, -546, -555, or -647 (1:500; Invitrogen). Tissue was rinsed for 15 minutes in PBS, repeated 3 times, and mounted in glycerol: PBS (9:1) and cover-slipped before confocal imaging. **Table 2** describes all antibodies and probes used in the study.

Confocal imaging. Three- or four-color fluorescence imaging was performed using a Zeiss LSM 700 or 900 laser scanning confocal microscope (Carl Zeiss Microscopy). *Z*-series images using 5x, 10×, 20×, 40×, or 63× objectives were obtained. Image processing and quantitative analyses were performed using IMARIS (Oxford Instruments), Volocity 3D image (Quorum Technologies Inc.), and Image J (NIH).

Resident and recruited macrophage counts. Resident macrophages (YFP+RFP+) and recruited monocytes and monocyte-derived macrophages (YFP+RFP-) were quantified in the spiral ganglion and the osseous spiral lamina (OSL) per cochlear section. Five-six mid-modiolar cochlear frozen sections, each 20 μm thick, were collected from sham-exposed and noise-exposed mice across eight time points: 0 hour (immediately), and 1, 3, 5, 7, 10, 15, and 30 days after noise exposure. Sections were immunolabeled for anti-GFP and anti-CD45 antibodies. Cells expressing YFP/GFP, RFP/tdTomato, and CD45 were quantified using IMARIS software and confirmed manually from 20x confocal images. Raw macrophage counts were reported for the OSL, while counts within spiral ganglion were normalized to the area of Rosenthal's canal for apex, middle, and base cochlear region and expressed as macrophage density per 1000 μm^2.

Fibrinogen Intensity measurement. Cochlear cryosections were immunolabeled for fibrinogen and imaged using an LSM 900 confocal microscope. The mean fluorescent intensity (MFI) was measured using the Image J software (NIH). A region of interest (ROI) was drawn around the site of fibrinogen signal, within Rosenthal's canal, lower spiral ligament, and spiral limbus. The area and mean fluorescence of the ROI were measured. Similarly, ROI was drawn over the region with no fibrinogen signal within the Rosenthal canal, lower spiral ligament, and spiral limbus to measure the background. The final fibrinogen fluorescent intensity is reported as the average MFI of the ROI subtracted from the average MFI of the background, keeping the area constant between each ROI and its respective background. **(Shihan et al., 2021)**

$$Fibrinogen\ intensity\ measurement = average\ MFI\ of\ ROI - average\ MFI\ of\ the\ background$$

Statistical analysis. All experiments were performed on at least three independent occasions (at least three biological replicates) and are indicated in the figure legends. Statistical analyses were performed via GraphPad

216 Software, Inc., La Jolla, CA. Data was checked for normality using the Shapiro–Wilk or Kolmogorov–Smirnov
217 Normality Test, and values are expressed as the means ± standard deviations (SDs) unless otherwise stated in
218 the figure legends. To determine statistical significance, we selected appropriate tests for each examined
219 parameter, including t tests for two-group comparisons and one- or two-way ANOVA for multigroup or
220 multifactorial analyses. A suitable *post hoc* analysis was conducted to determine specific between-group
221 differences for significant main effects or interactions identified through ANOVA. The results and corresponding
222 figure legends provide comprehensive statistical details, including error representations, sample sizes, and
223 experimental replication information. The results were considered statistically significant when the probability
224 values (*p*) were less than or equal to the predetermined significance threshold of 0.05. A Pearson's correlation
225 was used to assess the strength and direction of the relationship between fibrinogen deposition and the time
226 course of recruited macrophages in the noise-injured cochlea.
227

228 **RESULTS**

229 **1. Cre recombination efficiency in CX_3CR1-lineage leukocytes in adult mouse cochlea and blood.**

230 We have previously employed $CX_3CR1^{GFP/wt}$ reporter mice expressing enhanced green fluorescence protein
231 (EGFP) in cochlear macrophages to study their distribution and function in the injured cochlea **(Kaur et al., 2019,**
232 **KaurOhlemiller and Warchol, 2018, Kaur et al., 2015, Manickam et al., 2023)**. Although this mouse line aids
233 in visualizing macrophages in the injured cochlea, it does not distinguish RM from recruited Mo/Mo-M. Therefore,
234 it cannot be used to define the isolated roles of CX_3CR1-RM vs. recruited Mo-M in SGN survival after injury. To
235 address this, we have developed a fate mapping technique wherein CX_3CR1-RM and recruited Mo/Mo-M are
236 endogenously labeled with different fluorescent reporters. This was achieved by crossing mice bearing
237 tamoxifen-inducible Cre ($CX_3CR1^{YFP-CreER/YFP-CreER}$) to a red fluorescence protein (RFP) reporter mouse line
238 ($Rosa26^{RFP}$ *or* $R26^{RFP}$).(Yona et al., 2013, O'KorenMathew and Saban, 2016a, Plemel et al., 2020b) The progeny
239 of this cross, $CX_3CR1^{YFP-CreER/wt}$:$R26^{RFP}$ mice were injected with either tamoxifen or corn oil (vehicle) at postnatal
240 days 28 (P28) and 29 (P29) to label CX_3CR1 expressing cells (i.e., YFP+ cell) with RFP and were euthanized at
241 2 (P32) and 60 (P90) days post injection (Fig. 1A). Our first aim was to determine the Cre recombination
242 efficiency in CX_3CR1 lineage in both blood and cochlea of an adult mouse by flow cytometry and

243 immunohistochemistry, respectively. After 2 days of tamoxifen administration, we found 99% ± 0.39% of YFP+
244 RM in the cochlea and 40% ± 2.5% of YFP+ Mo in the blood expressed RFP. However, 60 days post-tamoxifen
245 injection, only cochlear RM maintained RFP expression (Fig. 1B-J); whereas RFP expression in blood-circulating
246 Mo was 'washed out' by 60 days, and only 2.5% ± 1.1% of these cells retained the expression (Fig. 1L, M). Thus,
247 at the 60-day time-point, cochlear RM and blood-circulating Mo/Mo-M exhibited a YFP+ RFP+ and YFP+ RFP−
248 phenotype, respectively. Tamoxifen injection did not affect the density of CD45-immunolabeled leukocytes in the
249 cochlea, and the leukocyte density was comparable to that of mice injected with vehicle (Fig. 1K). We also found
250 that in mice injected with vehicle (corn oil), 32% ± 3.3% of CX_3CR1-YFP+ CD45+ RM in the cochlea and 1.9% ±
251 1.0% of CD45+ CD11b+ Ly6G- monocytes in the blood co-expressed RFP, which is indicative of a leaky Cre
252 (Fig. 1B-E, M).

253 Our next aim was to determine the rate of turnover of cochlear RM in an adult mouse during steady state. To
254 address this question, the progeny $CX_3CR1^{YFP-CreER/wt}$:$R26^{RFP}$ mice were injected with tamoxifen or corn oil and
255 euthanized at various time points post injection (Fig. 2A). Examination of the recombined CX_3CR1-expressing
256 RM (i.e., YFP+ RFP+ cells) in different cochlear compartments such as the sensory epithelium, Rosenthal's
257 canal or spiral ganglion and lateral wall for more than one year indicate that their turnover rate is slower than the
258 blood circulating Mo/Mo-M (typically ranging from 1 to 3 days) **(Gonzalez-Mejia and Doseff, 2009, WHITELAW**
259 **and Bell, 1966)** but similar to the long-lived self-renewing microglia (brain resident macrophages) **(Ajami et al.,**
260 **2007, Xu et al., 2007)** (Fig. 2B-F). Notably, a few recruited Mo/Mo-M (i.e., YFP+ RFP- cells) were observed
261 under steady state, particularly in Rosenthal's canal and spiral ligament as a function of aging, along with a trend
262 of an increase in macrophage numbers in aged versus young cochlea (Fig. 2E, F).

263

264 **2. Fate mapping with $CX_3CR1^{YFP-CreER/wt}$:$R26^{RFP}$ mice distinguishes CX_3CR1-expressing RM and**
265 **recruited Mo/Mo-M in the cochlea following acoustic trauma.**

266 Previously, we have reported a unique spatiotemporal pattern of macrophage migration into the noise-injured
267 cochlea, where macrophages migrate immediately and temporarily towards the damaged sensory epithelium,
268 followed by a sustained increase in macrophage numbers in the spiral ganglion **(KaurOhlemiller and Warchol,**
269 **2018, Kaur et al., 2015)**. However, it is unclear whether this increase in macrophage numbers in the ganglion is

270 due to local proliferation of RM or recruitment of Mo from blood circulation and their differentiation into Mo-M or
271 both. To address this, we exposed the “washed out” mice to an acoustic trauma for 2 hours at a noise level of
272 112 dB SPL at 8-16 kHz that causes permanent hearing loss, and damage to hair cells and spiral ganglion
273 neurons **(Hirose et al., 2005)**. Cochleae were analyzed immediately and at 1, 3, 5, 7, 10, 15, 30 days post
274 acoustic trauma (Fig. 3A). We observed a YFP+ RFP+ population consistent with cochlear RM and a YFP+
275 RFP− population consistent with recruited Mo/Mo-M cells in the spiral ganglion by 7 days post exposure (Fig.
276 3B, bottom panel). In contrast, sham-exposed mice only contained YFP+ RFP+ RM (Fig. 3B, top panel). Next,
277 we quantified the densities of YFP+ RFP+ RM and YFP+ RFP− recruited Mo/Mo-M in the neuronal region, i.e.,
278 spiral ganglion and spiral lamina, as a function of days post-exposure (DPNE) to determine their spatiotemporal
279 distribution in the noise-injured cochlea. At 1 DPNE, the density of YFP+ RFP+ RM significantly decreased in
280 the spiral ganglion and concurrently increased in the spiral lamina in the apex, middle, and basal cochlear turns
281 when compared to densities in the sham-exposed and 0-day noise-exposed mice. Remarkably, by 3 DPNE, the
282 density of YFP+ RFP+ RM in the spiral ganglion was restored to the levels as observed in the sham-exposed
283 mice, and their numbers peaked by 5-7 DPNE and then returned to baseline by 30 DPNE in all cochlear turns.
284 Similarly, the density of YFP+ RFP+ RM also peaked in the spiral lamina at around 3-7 DPNE in all three cochlear
285 turns, after which they declined to the levels observed in the sham-exposed mice (Fig. 3C, D). YFP+ RFP−
286 recruited Mo/Mo-M were rarely seen in and around the spiral ganglion and spiral lamina in the sham-exposed
287 and 0-day noise-exposed cochlea. At 1 DPNE (i.e., same time when the numbers of YFP+ RFP+ RM are
288 decreased in the spiral ganglion), YFP+ RFP− recruited Mo/Mo-M were found to be present in both spiral
289 ganglion and spiral lamina. By 3-7 DPNE, the density of YFP+ RFP− recruited Mo/Mo-M increased in all three
290 cochlear turns, with significantly higher densities in the apical ganglion and lamina, after which their numbers
291 started to wane. By 30 DPNE, few (around 1-2) YFP+ RFP− recruited Mo/Mo-M were still observed in the spiral
292 lamina but rarely in the spiral ganglion of all three cochlear turns (Fig. 3C, D). In addition to the neuronal region,
293 Mo/Mo-M were also detected around the sensory epithelium and in the spiral ligament (primary site for
294 macrophage accumulation), but not in the stria vascularis of the noise-injured cochlea (Fig. 4A-D).
295

296 **3. Recruited Mo/Mo-M originate from bone marrow-derived circulating monocytes and are**
297 **morphologically indistinguishable from cochlear RM undergoing *in situ* proliferation following**
298 **acoustic trauma.**

299 Recruited macrophages into an injured tissue originate from bone marrow (BM) precursors, specifically,
300 circulating monocytes that express high levels of Ly6C, CCR2, Ms4a3, and CD62L (L-selectin) and low levels
301 of CX_3CR1 **(CotechiniAtallah and Grossman, 2021, Gordon and Plüddemann, 2017, Liu et al., 2019, Yang**
302 **et al., 2014)**. We immunolabeled the cochlear cryosections for the markers mentioned above to verify that the
303 recruited Mo/Mo-M in the noise-injured cochlea originate from BM-derived circulating monocytes. Out of the four
304 antibodies tested (Ly6C, CCR2, Ms4a3, and CD62L (L-selectin)), only two worked in our hands (Ly6C and
305 CCR2). The data presented in Figure 5 show that the recruited Mo/Mo-M (YFP+ RFP−) expressed Ly6C and
306 CCR2, confirming that these cells are derived from circulating monocytes (Fig. 5A, B). Unexpectedly, RM in the
307 ganglion also displayed the expression of Ly6C (Fig. 5B) but were negative for CCR2 in the noise-injured
308 cochlea.

309 Morphometric analysis of YFP+ RFP+ RM and YFP+ RFP− Mo/Mo-M at 1- and 7-days post noise exposure
310 displayed no significant morphological differences between the two cell types, suggesting that morphology is a
311 poor indicator to distinguish CX_3CR1-expressing resident and recruited macrophages in the noise-injured
312 cochlea (Fig. 6A, B). Notably, recruited Mo transform from round or less ramified at 1 DPNE to being more
313 ramified-like macrophages by 7 DPNE, suggesting that the recruited Mo may eventually differentiate into
314 cochlear RM (Fig. 6A, B).

315 Microglia (brain RM) undergo local proliferation after injury **(Plemel et al., 2020a)**. Thus, to determine if
316 acoustic trauma induces RM expansion in the spiral ganglion (as seen in Fig. 3) due to local proliferation and
317 limited death, cochleae were immunolabeled for Ki-67 (cell proliferation marker) and cleaved caspase-3 (CC3,
318 key effector of apoptosis), and the numbers of Ki67+ and CC3+ RM and Mo/Mo-M were quantified. Probing for
319 cleaved caspase-3 showed no evidence for RM and Mo/Mo-M undergoing apoptosis (Fig. 7A). As expected,
320 immunolabeling for Ki67 showed proliferating YFP+ RFP− Mo/Mo-M only at 1 DPNE (i.e., time when these cells
321 infiltrate the spiral ganglion) in the middle and basal spiral ganglion as they typically proliferate during the process
322 of extravasation from the blood into the noise-injured cochlea (Fig. 7B, C). Unexpectedly, Ki67 immunolabeled

323 YFP+ RFP+ RM were observed at 3 DPNE in the spiral ganglion of all three turns, indicating that RM undergo
324 *in-situ* proliferation after acoustic trauma (Fig. 7B, C). These and the above data imply that the increase in overall
325 macrophage numbers in the spiral ganglion and lamina after acoustic trauma results from both *in situ* proliferation
326 of RM and recruitment of blood-circulating Mo/Mo-M. Although blood-derived macrophages acutely infiltrated
327 the spiral ganglion, resident macrophages progressively monopolized the ganglion after noise trauma, likely due
328 to proliferation.
329

330 **4. Recruitment of CX_3CR1-expressing Mo/Mo-M into the spiral ganglion is associated with vascular**
331 **damage and fibrinogen extravasation from blood into the cochlea after acoustic trauma.**

332 The blood labyrinth barrier (BLB) is a network of specialized capillaries that normally limits the passage of
333 substances, including toxins, proteins, pathogens, and immune cells, between the bloodstream and inner ear
334 fluids, which is crucial for the maintenance of cochlear homeostasis. Inflammation, noise trauma, ototoxicity, and
335 aging produce changes in the BLB, resulting in increased vascular permeability, also known as "leaky
336 vasculature"**(Hirose et al., 2014, Shi, 2016)**. Such leaky vasculature may allow the blood-circulating immune
337 cells to enter the compromised cochlea. Therefore, we wanted to determine if recruitment of CX_3CR1-expressing
338 Mo/Mo-M in the neuronal region occurs either before, at the same time, or after the breakdown of the BLB in the
339 noise-injured cochlea. To address this, we immunolabeled the cochlear sections from the sham-exposed and
340 noise-exposed "washed out" mice with fibrinogen antibody. Fibrinogen is a pleiotropic blood-clotting protein that
341 extravasates into the nervous system after injury or disease associated with vascular damage or blood-brain
342 barrier (BBB) breakdown, thus serving as a marker of BBB disruption **(RyuDavalos and Akassoglou, 2009)**.
343 The data shows fibrinogen immunolabeling inside the cochlear labyrinth after an acoustic trauma of 112 dB SPL
344 for 2 hours at 8-16 kHz octave band, suggesting vascular damage or compromised BLB following such injury
345 (Fig. 8A). Fibrinogen extravasation and deposition was observed inside and around the spiral ganglion, in the
346 spiral limbus, as well as in the lower spiral ligament and stria vascularis, which are predominantly vascularized
347 cochlear regions, suggesting vascular damage after exposure (Fig. 8A). Compared to the uninjured cochlea, the
348 fluorescence intensity of fibrinogen increased by 1-3 DPNE primarily in the middle and basal spiral ganglion and
349 spiral limbus, and in the lower spiral ligament and was decreased by 10 DPNE (Fig. 8A, C). To determine if the

350 recruitment of blood-circulating Mo/Mo-M in the SGN is associated with a leaky vasculature after acoustic
351 trauma, a correlation analysis was performed between fibrinogen intensity and recruited Mo/Mo-M density in the
352 spiral ganglion at 0, 1, 3, 5, 7, and 10 days after noise exposure. The analysis revealed a strong and positive
353 correlation between fibrinogen intensity and macrophage recruitment in the middle ganglion (Pearson correlation
354 coefficient, r = 0.8), whereas no correlation was found in the base and apex ganglia of the noise-injured cochlea
355 (r = 0.16 and -0.09, base and apex, respectively) (Fig. 8D). These data offer a novel probe, fibrinogen, as a blood
356 marker for cochlear vascular damage after acoustic trauma and indicate that recruitment of circulating Mo/Mo-
357 M in the cochlea follows vascular damage.
358

359 **DISCUSSION**

360 Our novel work involves the use of fate mapping with *$CX_3CR1^{YFP-CreER/wt}$:$R26^{RFP}$* mice to address unresolved
361 questions concerning the presence of bona fide resident versus recruited macrophages and their phenotypic
362 differences and similarities in the injured cochlea. Distinguishing resident from recruited macrophages in the
363 injured cochlea has proven to be challenging. Indeed, recruited classical Mo can be resolved phenotypically
364 acutely after injury as they express Ly6C and CCR2, but not F4/80 or Iba-1 **(Pan et al., 2024, Shin et al., 2022)**
365 . However, differentiated Mo-derived macrophages (Mo-M) may overlap phenotypically with RM because both
366 express CX_3CR1, F4/80, or Iba-1, but non- or reduced expression of Ly6C **(Shin et al., 2022)**. Using genetic
367 reporter mice such as *$CX_3CR1^{GFP/wt}$* mice to identify CX_3CR1-expressing RM in the injured cochlea can be
368 misleading, because recruited Mo/Mo-M also express CX_3CR1 **(Jung et al., 2000, Molawi et al., 2014, Yona et**
369 **al., 2013, Zigmond et al., 2012)**, as shown in the central nervous system (CNS) **(Kierdorf et al., 2013, Shechter**
370 **et al., 2013)**. A similar concern is also with using *$CCR2^{RFP/wt}$* mice to identify Mo and Mo-derived cells, as fully
371 differentiated Mo-M downregulate their expression of CCR2 to negligible levels that are similar to RM, such as
372 microglia in the brain **(GreterLelios and Croxford, 2015, Saederup et al., 2010)**. Generating GFP bone marrow
373 chimeras is a commonly used non-genetic approach to discern cochlear RM from recruited Mo and Mo-derived
374 cells under steady state, or during injury **(Lang et al., 2016, Okano et al., 2008, Sato et al., 2008, Shi, 2010)**.
375 However, this method is also confounded since whole-body irradiation/bone marrow transplantation itself leads
376 to recruitment of bone marrow-derived cells into the tissue **(Ajami et al., 2007, Chen et al., 2012, Okano et al.,**

377 **2008, Xu et al., 2007)**. Parabiosis bypasses this problem **(Ajami et al., 2007)** but does not reach full chimerism
378 in the periphery and is not widely used for multiple reasons **(Kierdorf et al., 2013)**, including significant technical
379 challenges.

380 In the current study, we found that the *CX$_3$CR1$^{YFP-CreER/wt}$:R26^{RFP}* mouse induces *loxP* recombination in
381 cochlear RM (~ 30%) and blood myeloid cells (~ 2%) in the absence of tamoxifen. Such *CreER* leakiness has
382 also been reported in microglia of *CX$_3$CR1^{CreER}* mouse lines **(Fonseca et al., 2017, Stowell et al., 2019, Van**
383 **Hove et al., 2020)**. Nevertheless, this *CreER* leakiness did not significantly hinder the interpretation of the data
384 regarding cochlear RM turnover under steady state or recruitment, distribution, and fate of RM, and Mo/Mo-M in
385 the aging or noise-injured cochlea. This is because of the use of the 'washed out' *CX$_3$CR1$^{YFP-CreER/wt}$:R26^{RFP}*
386 mice in which, upon tamoxifen injection, nearly 100% of cochlear RM recombined, whereas blood myeloid cells
387 lose the recombination by 60 days, as they are short-lived and turn over quickly due to ongoing, lifelong
388 hematopoiesis. Besides *CX$_3$CR1*, cochlear RM also expresses *Tmem119* and *P2ry12* **(Bassiouni et al., 2023,**
389 **Chiot et al., 2024)**, and inducible *Cre* lines, including *Tmem119^{CreER}* and *P2ry12^{CreER}* are available commercially.
390 A comparative analysis of these inducible lines for *Cre* recombination with and without tamoxifen, as well as
391 specificity (resident vs. recruited), is needed in the future to inform on the caveats and benefits of all tools for
392 reliable manipulation of cochlear macrophage function *in vivo* and development of macrophage-based therapies
393 for acquired sensorineural hearing loss. Studies using bone marrow chimeras have reported that the turnover of
394 cochlear RM is slow and progressive under steady state **(Okano et al., 2008, Shi, 2010)**. Our findings with the
395 *CX$_3$CR1$^{YFP-CreER/wt}$:R26^{RFP}* fate mapping tool corroborate with these studies. They reveal that while RM
396 represented a stable population in the cochlea, a slow and progressive contribution of blood-circulating Mo/Mo-
397 M to the macrophage pool occurs in the spiral ganglion and lateral wall, starting around 5 months of age. With
398 respect to turnover rates, our findings imply that cochlear RM have characteristics as of resident
399 macrophages/microglia in the brain and retina that are long-lived **(Ajami et al., 2007, Hess et al., 2004, Simard**
400 **et al., 2006, Xu et al., 2007)** and not as peripheral tissue-resident macrophages that turnover quickly **(Gonzalez-**
401 **Mejia and Doseff, 2009, Naito et al., 1997)**. The mechanisms that regulate the maintenance of cochlear RM
402 remain to be elucidated and are subject to future investigation.

403 Our data with acoustic trauma in the 'washed out' *$CX_3CR1^{YFP-CreER/wt}$:$R26^{RFP}$* mice revealed interesting spatial
404 and temporal distribution patterns for cochlear RM and Mo/Mo-M, particularly in the neuronal region. A day after
405 acoustic trauma, the decreased density of RM in the spiral ganglion and their simultaneous increase in the spiral
406 lamina across all cochlear turns validate our previous work with a 2-hour exposure at 120 dB SPL reported in
407 Kaur et al., 2018. Reduced number of RM in the spiral ganglion is not due to apoptosis and may suggest that
408 RM in the spiral ganglion migrate towards the spiral lamina and sensory epithelium immediately following
409 acoustic trauma. During the same time after exposure, Mo/Mo-M infiltrate the empty niche in the middle and
410 base spiral ganglion. The molecular signals that allow local migration of RM from the ganglion towards the lamina
411 and that cause Mo/Mo-M extravasation from the blood into the ganglion remain unknown. We have previously
412 reported the fractalkine (CX_3CL1) molecule as a putative chemoattractant for macrophages that also regulate
413 their numbers in the injured cochlea **(KaurOhlemiller and Warchol, 2018, Kaur et al., 2015, Manickam et al.,**
414 **2024)**. Additional studies are needed to determine if fractalkine is a chemoattractant for RM or Mo/Mo-M or both
415 in the injured cochlea. Unexpectedly, the reduced numbers of RM (YFP+RFP+) in the spiral ganglion started to
416 recover by 3 days and were restored to baseline by 1 week following acoustic trauma. One reason for this effect
417 would be the *in situ* proliferation of the remaining cochlear RM. To this end, our data establishes for the first time
418 the presence of Ki67-positive cochlear RM (YFP+RFP+) at 3 days post-noise exposure, which may contribute
419 to the pool of increased numbers of RM. Another explanation could be that recruited Mo (YFP+ RFP-) in the
420 ganglion immediately and 1 day after exposure quickly differentiate into RM, and thus increase the density of
421 RM. Indeed, **(Shin et al., 2022)** have reported that after acoustic overstimulation, monocytes infiltrated the lower
422 spiral ligament within 2 days, followed by transformation into macrophages at 3-5 days based on CX_3CR1
423 upregulation and Ly6C downregulation immunolabeling. Nonetheless, in the fate mapping 'washed out'
424 *$CX_3CR1^{YFP-CreER/wt}$:$R26^{RFP}$* mice, recruited Mo/Mo-M (YFP+ RFP-) in the spiral ganglion or lower spiral ligament
425 did not show the expression for RFP, in case they differentiated into RM. While our data show that the recruited
426 Mo/Mo-M expressed classical monocyte markers, Ly6C and CCR2, their further characterization for expression
427 of unique markers for RM, including Iba-1, F4/80, CD64, and MHC-II, is vital to resolve this issue. Besides
428 recruited Mo/Mo-M (YFP+ RFP-), Ly6C expression was also observed in RM (YFP+RFP+) in the spiral ganglion
429 at 3 days post-noise exposure. Such Ly6C expression on both resident and recruited macrophages could be

430 associated with an inflammatory response or phenotype during the early stages of cochlear injury. Whether these
431 Ly6C-expressing RM switch to non- or low-Ly6C expression at later stages of injury remains to be determined.
432 **(Hirose et al., 2005)** reported that an increase in macrophages in the noise-injured cochlea arises from infiltration
433 of inflammatory cells from the vasculature as opposed to mitotic division of resident phagocytes. Yet, our findings
434 using the fate mapping across different days after acoustic trauma have shed new light on the basic
435 understanding of the mechanisms of the increase in macrophage numbers in the spiral ganglion in the noise-
436 injured cochlea, which involves both recruitment of blood-circulating Mo and *in situ* proliferation of cochlear RM.
437 Fibrinogen, also known as coagulation factor I, is abundant in the blood and functions in the coagulation
438 cascade, creating polymers of fibrin. Fibrinogen leakage into the brain or retina is a hallmark of a compromised
439 blood-brain or blood-retina barrier in multiple sclerosis **(DavalosMahajan and Trapp, 2019)**, Alzheimer's **(Ryu**
440 **and McLarnon, 2008),** and diabetic retinopathy patients **(Muratalshibashi and Inomata, 1992)**. Similarly, it has
441 been reported that there is a strong relationship between plasma fibrinogen levels and the pathogenesis of
442 sudden sensorineural hearing loss **(Lu et al., 2008)**. In this study, we show that fibrinogen extravasation and
443 deposition occur in the cochlea as early as one day after acoustic trauma in areas closely associated with blood
444 vessels, including the spiral ligament, the spiral limbus, and the spiral ganglion. Other investigators have also
445 shown leaky cochlear vessels with fluorescent tracers such as serum albumin-FITC or serum protein IgG in
446 noise-exposed animals **(Yang et al., 2011, Zhang et al., 2013)**. However, fibrinogen is a large glycoprotein with
447 a molecular weight of 340 kDa relative to 65 kDa of albumin or 150 kDa of IgG, highlighting the magnitude of
448 BLB damage after a 2-hour exposure to a noise level of 112 dB SPL. Remarkably, such fibrinogen deposition
449 strongly correlated with the time course of recruitment of blood-circulating Mo/Mo-M primarily in the spiral
450 ganglion and with perivascular clustering of activated macrophages in the ligament, limbus, and spiral ganglion
451 of the noise-injured cochlea. This suggests that the dynamics of recruitment of circulating Mo/Mo-M is
452 determined by leaky vasculature. Studies have revealed structural and molecular changes in the BLB after
453 acoustic trauma that result in destabilization of the barrier and thus cause leaky vasculature. These changes
454 include alterations in the location of pericytes, activation of perivascular macrophages, production of PEDF by
455 activated macrophages that results in downregulation of barrier tight-junction and adherent-junction associated
456 proteins, and vascular leakage **(Shi, 2009, Yang et al., 2011, Zhang et al., 2013, Zhang et al., 2012)**. The

process by which blood-circulating monocytes are recruited into an injured tissue is called chemotaxis, which is the directed movement of cells in response to chemokines. Several adhesion molecules and chemoattractants, including ICAM-1, MCP-5 (CCL12), MCP-1 (CCL2), and MIP-1beta (CCL4), have been found to be upregulated after acoustic trauma **(Frye et al., 2017, Sautter et al., 2006, TanThorne and Vlajkovic, 2016, Tornabene et al., 2006)**. Chemokine CCL2 and its primary receptor, CCR2, are the most widely validated effector of monocyte chemotaxis *in vivo* **(Ransohoff et al., 2002, Rollins, 1996)**. However, it has been shown that the number of cochlear macrophages remains unchanged after acoustic trauma in the absence of CCL2 or CCR2 **(Sautter et al., 2006).** Investigations on the specific chemoattractants that recruit Mo/Mo-M into the noise-injured cochlea and determining their molecular phenotypes and precise functions after acoustic trauma are underway.

In conclusion, this study demonstrates for the first time the use of fate-mapping as a tool to clearly distinguish cochlear resident macrophages from blood-circulating recruited monocytes and monocyte-derived macrophages in normal, aging, and noise-injured cochleae. Our data confirms that cochlear RM turnover occurs at a slower rate than the peripheral leukocytes. In addition, biological aging or acoustic trauma recruit blood-circulating Mo into the cochlea through a leaky/permeable BLB, which are morphologically similar to RM. Importantly, besides the recruitment of Mo and their differentiation into tissue macrophages (Mo-M), self-renewal of RM also contributes to the overall increase in the numbers of macrophages in the cochlea after acoustic trauma (Fig. 9).

ABBREVIATIONS

RM: Resident macrophages

Mo: Monocytes

Mo-M: Monocyte-derived macrophages

YFP: Yellow fluorescent protein

GFP: Green fluorescent protein

RFP: Red fluorescent protein

IHC: Inner hair cell

SGN: Spiral ganglion neuron

OSL: Osseous spiral lamina

SE: Sensory epithelium

dB: Decibel

SPL: Sound pressure level

kHz: Kilohertz

kDa: Kilodalton

DPNE: Days post noise exposure

BLB: Blood labyrinth barrier

REFERENCES

Ajami, B., Bennett, J. L., Krieger, C., Tetzlaff, W. & Rossi, F. M. V. 2007. Local self-renewal can sustain CNS microglia maintenance and function throughout adult life. *Nature Neuroscience,* 10**,** 1538-1543.

Bassiouni, M., Smorodchenko, A., Olze, H. & Szczepek, A. J. 2023. Identification and Characterization of TMEM119-Positive Cells in the Postnatal and Adult Murine Cochlea. *Brain Sciences,* 13**,** 516-516.

Chen, M., Zhao, J. W., Luo, C., Pandi, S. P. S., Penalva, R. G., Fitzgerald, D. C. & Xu, H. P. 2012. Para-inflammation-mediated retinal recruitment of bone marrow-derived myeloid cells following whole-body irradiation is CCL2 dependent. *Glia,* 60**,** 833-842.

Chiot, A., Felgner, M. J., Brownell, D., Rott, K. H., Bogachuk, A., Rosmus, D.-D., Masuda, T., Ching, A., Atkinson, P. J., Prinz, M., Sachs, K., Cheng, A. G., Wieghofer, P. & Ajami, B. 2024. Single-cell, spatial, and fate-mapping analyses uncover niche dependent diversity of cochlear myeloid cells. *bioRxiv***,** 2024.10.30.621184-2024.10.30.621184.

Cotechini, T., Atallah, A. & Grossman, A. 2021. Tissue-Resident and Recruited Macrophages in Primary Tumor and Metastatic Microenvironments: Potential Targets in Cancer Therapy. *Cells,* 10.

Davalos, D., Mahajan, K. R. & Trapp, B. D. 2019. Brain fibrinogen deposition plays a key role in MS pathophysiology – Yes. *Multiple Sclerosis Journal,* 25**,** 1434-1435.

Dong, Y., Zhang, C., Frye, M., Yang, W., Ding, D., Sharma, A., Guo, W. & Hu, B. H. 2018. Differential fates of tissue macrophages in the cochlea during postnatal development. *Hearing Research,* 365**,** 110-126.

Fonseca, M. I., Chu, S. H., Hernandez, M. X., Fang, M. J., Modarresi, L., Selvan, P., Macgregor, G. R. & Tenner, A. J. 2017. Cell-specific deletion of C1qa identifies microglia as the dominant source of C1q in mouse brain. *Journal of Neuroinflammation,* 14**,** 48-48.

Frye, M. D., Yang, W., Zhang, C., Xiong, B. & Hu, B. H. 2017. Dynamic activation of basilar membrane macrophages in response to chronic sensory cell degeneration in aging mouse cochleae. *Hearing Research,* 344**,** 125-134.

Geissmann, F., Manz, M. G., Jung, S., Sieweke, M. H., Merad, M. & Ley, K. 2010. Development of monocytes, macrophages, and dendritic cells. *Science,* 327**,** 656-661.

Ginhoux, F. & Guilliams, M. 2016. Tissue-Resident Macrophage Ontogeny and Homeostasis. *Immunity,* 44**,** 439-449.

Ginhoux, F. & Jung, S. 2014. Monocytes and macrophages: developmental pathways and tissue homeostasis. *Nature Reviews Immunology,* 14**,** 392-404.

Goldmann, T., Wieghofer, P., Müller, P. F., Wolf, Y., Varol, D., Yona, S., Brendecke, S. M., Kierdorf, K., Staszewski, O., Datta, M., Luedde, T., Heikenwalder, M., Jung, S. & Prinz, M. 2013. A new type of microglia gene targeting shows TAK1 to be pivotal in CNS autoimmune inflammation. *Nature Neuroscience,* 16**,** 1618-1626.

Gonzalez-Mejia, M. E. & Doseff, A. I. 2009. Regulation of monocytes and macrophages cell fate. *Frontiers in Bioscience,* 14**,** 2413-2431.

Gordon, S. & Plüddemann, A. 2017. Tissue macrophages: heterogeneity and functions. *Bmc Biology,* 15.

Greter, M., Lelios, I. & Croxford, A. L. 2015. Microglia versus myeloid cell nomenclature during brain inflammation. *Frontiers in Immunology,* 6.

Hess, D. C., Abe, T., Hill, W. D., Studdard, A. M., Carothers, J., Masuya, M., Fleming, P. A., Drake, C. J. & Ogawa, M. 2004. Hematopoietic origin of microglial and perivascular cells in brain. *Experimental Neurology,* 186**,** 134-144.

Hirose, K., Discolo, C. M., Keasler, J. R. & Ransohoff, R. 2005. Mononuclear phagocytes migrate into the murine cochlea after acoustic trauma. *Journal of Comparative Neurology,* 489**,** 180-194.

Hirose, K., Hartsock, J. J., Johnson, S., Santi, P. & Salt, A. N. 2014. Systemic Lipopolysaccharide Compromises the Blood-Labyrinth Barrier and Increases Entry of Serum Fluorescein into the Perilymph. *Jaro-Journal of the Association for Research in Otolaryngology,* 15**,** 707-719.

Hosoya, M., Kitama, T., Shimanuki, M. N., Nishiyama, T., Oishi, N., Okano, H. & Ozawa, H. 2023. Distribution of macrophages in the developing cochlea of the common marmoset, a primate model animal. *Frontiers in Immunology,* 14.

Jung, S. 2018. Macrophages and monocytes: of tortoises and hares. *Nature Reviews Immunology 2017 18:2,* 18**,** 85-86.

Jung, S., Aliberti, J., Graemmel, P., Sunshine, M. J., Kreutzberg, G. W., Sher, A. & Littman, D. R. 2000. Analysis of Fractalkine Receptor CX3CR1 Function by Targeted Deletion and Green Fluorescent Protein Reporter Gene Insertion. *Molecular and Cellular Biology,* 20**,** 4106-4114.

Kaur, T., Clayman, A. C., Nash, A. J., Schrader, A. D., Warchol, M. E. & Ohlemiller, K. K. 2019. Lack of fractalkine receptor on macrophages impairs spontaneous recovery of ribbon synapses after moderate noise trauma in c57bl/6 mice. *Frontiers in Neuroscience,* 13**,** 463900-463900.

Kaur, T., Ohlemiller, K. K. & Warchol, M. E. 2018. Genetic disruption of fractalkine signaling leads to enhanced loss of cochlear afferents following ototoxic or acoustic injury. *Journal of Comparative Neurology,* 526**,** 824-835.

Kaur, T., Zamani, D., Tong, L., Rube, E. W., Ohlemiller, K. K., Hirose, K. & Warchol, M. E. 2015. Fractalkine Signaling Regulates Macrophage Recruitment into the Cochlea and Promotes the Survival of Spiral Ganglion Neurons after Selective Hair Cell Lesion. *Journal of Neuroscience,* 35**,** 15050-15061.

Kierdorf, K., Katzmarski, N., Haas, C. A. & Prinz, M. 2013. Bone Marrow Cell Recruitment to the Brain in the Absence of Irradiation or Parabiosis Bias. *PLoS ONE,* 8.

Lang, H., Nishimoto, E., Xing, Y., Brown, L. S. N., Noble, K. V., Barth, J. L., Larue, A. C., Ando, K. & Schulte, B. A. 2016. Contributions of mouse and human hematopoietic cells to remodeling of the adult auditory nerve after neuron loss. *Molecular Therapy,* 24**,** 2000-2011.

Liu, W., Molnar, M., Garnham, C., Benav, H. & Rask-Andersen, H. 2018. Macrophages in the human cochlea: Saviors or predators-A study using super-resolution immunohistochemistry. *Frontiers in Immunology,* 9**,** 334425-334425.

Liu, Z. Y., Gu, Y. Q., Chakarov, S., Bleriot, C., Kwok, I., Chen, X., Shin, A., Huang, W. J., Dress, R. J., Dutertre, C. A., Schlitzer, A., Chen, J. M., Ng, L. G., Wang, H. L., Liu, Z. D., Su, B. & Ginhoux, F. 2019. Fate Mapping via Ms4a3-Expression History Traces Monocyte-Derived Cells. *Cell,* 178**,** 1509-+.

Lu, Y. Y., Jin, Z., Tong, B. S., Yang, J. M., Liu, Y. H. & Duan, M. 2008. A clinical study of microcirculatory disturbance in Chinese patients with sudden deafness. *Acta Oto-Laryngologica,* 128**,** 1168-1172.

Manickam, V., Gawande, D. Y., Stothert, A. R., Clayman, A. C., Batalkina, L., Warchol, M. E., Ohlemiller, K. K. & Kaur, T. 2023. Macrophages Promote Repair of Inner Hair Cell Ribbon Synapses following Noise-Induced Cochlear Synaptopathy. *Journal of Neuroscience,* 43**,** 2075-2089.

Manickam, V., Maity, S., Murali, S. V., Gawande, D. Y., Stothert, A. R., Batalkina, L., Cardona, A. E. & Kaur, T. 2024. Local delivery of soluble fractalkine (CX3CL1) peptide restores ribbon synapses after noise-induced cochlear synaptopathy. *Frontiers in Cellular Neuroscience,* 18**,** 1486740-1486740.

Molawi, K., Wolf, Y., Kandalla, P. K., Favret, J., Hagemeyer, N., Frenzel, K., Pinto, A. R., Klapproth, K., Henri, S., Malissen, B., Rodewald, H. R., Rosenthal, N. A., Bajenoff, M., Prinz, M., Jung, S. & Sieweke, M. H. 2014. Progressive replacement of embryo-derived cardiac macrophages with age. *Journal of Experimental Medicine,* 211**,** 2151-2158.

580 Murata, T., Ishibashi, T. & Inomata, H. 1992. Immunohistochemical detection of extravasated fibrinogen (fibrin)
581 in human diabetic retina. *Graefe's Archive for Clinical and Experimental Ophthalmology,* 230**,** 428-431.
582 Naito, M., Umeda, S., Takahashi, K. & Shultz, L. D. 1997. Macrophage differentiation and granulomatous
583 inflammation in osteopetrotic mice (op/op) defective in the production of CSF-1. *Molecular Reproduction*
584 *and Development,* 46**,** 85-91.
585 O'koren, E. G., Mathew, R. & Saban, D. R. 2016a. Fate mapping reveals that microglia and recruited monocyte-
586 derived macrophages are definitively distinguishable by phenotype in the retina. *Sci Rep,* 6**,** 20636.
587 O'koren, E. G., Mathew, R. & Saban, D. R. 2016b. Fate mapping reveals that microglia and recruited monocyte-
588 derived macrophages are definitively distinguishable by phenotype in the retina. *Scientific Reports,* 6**,**
589 20636-20636.
590 O'malley, J. T., Nadol, J. B. & Mckenna, M. J. 2016. Anti CD163+, Iba1+, and CD68+ Cells in the Adult Human
591 Inner Ear: Normal Distribution of an Unappreciated Class of Macrophages/Microglia and Implications for
592 Inflammatory Otopathology in Humans. *Otology & neurotology : official publication of the American*
593 *Otological Society, American Neurotology Society [and] European Academy of Otology and Neurotology,*
594 37**,** 99-108.
595 Okano, T., Nakagawa, T., Kita, T., Kada, S., Yoshimoto, M., Nakahata, T. & Ito, J. 2008. Bone marrow-derived
596 cells expressing Iba1 are constitutively present as resident tissue macrophages in the mouse cochlea.
597 *Journal of Neuroscience Research,* 86**,** 1758-1767.
598 Pan, J., Wang, K., Qu, J., Chen, D., Chen, A., You, Y., Tang, J. & Zhang, H. 2024. Activated tissue-resident
599 macrophages contribute to hair cell insults in noise-induced hearing loss in mice. *Communications*
600 *Biology 2024 7:1,* 7**,** 1-13.
601 Parkhurst, C. N., Yang, G., Ninan, I., Savas, J. N., Yates, J. R., Lafaille, J. J., Hempstead, B. L., Littman, D. R.
602 & Gan, W. B. 2013. Microglia Promote Learning-Dependent Synapse Formation through Brain-Derived
603 Neurotrophic Factor. *Cell,* 155**,** 1596-1609.
604 Plemel, J. R., Stratton, J. A., Michaels, N. J., Rawji, K. S., Zhang, E., Sinha, S., Baaklini, C. S., Dong, Y., Ho,
605 M., Thorburn, K., Friedman, T. N., Jawad, S., Silva, C., Caprariello, A. V., Hoghooghi, V., Yue, J., Jaffer,
606 A., Lee, K., Kerr, B. J., Midha, R., Stys, P. K., Biernaskie, J. & Wee Yong, V. 2020a. Microglia response
607 following acute demyelination is heterogeneous and limits infiltrating macrophage dispersion. *Science*
608 *Advances,* 6.
609 Ransohoff, R. M., Wei, T., Pavelko, K. D., Lee, J. C., Murray, P. D. & Rodriguez, M. 2002. Chemokine expression
610 in the central nervous system of mice with a viral disease resembling multiple sclerosis:: Roles of CD4
611 and CD8 T cells and viral persistence. *Journal of Virology,* 76**,** 2217-2224.
612 Rollins, B. J. 1996. Monocyte chemoattractant protein 1: A potential regulator of monocyte recruitment in
613 inflammatory disease. *Molecular Medicine Today,* 2**,** 198-204.
614 Ryu, J. K., Davalos, D. & Akassoglou, K. 2009. Fibrinogen signal transduction in the nervous system. *Journal of*
615 *Thrombosis and Haemostasis,* 7**,** 151-154.
616 Ryu, J. K. & Mclarnon, J. G. 2008. A leaky blood–brain barrier, fibrinogen infiltration and microglial reactivity in
617 inflamed Alzheimer's disease brain. *Journal of Cellular and Molecular Medicine,* 13**,** 2911-2911.
618 Saederup, N., Cardona, A. E., Croft, K., Mizutani, M., Cotleur, A. C., Tsou, C. L., Ransohoff, R. M. & Charo, I. F.
619 2010. Selective Chemokine Receptor Usage by Central Nervous System Myeloid Cells in CCR2-Red
620 Fluorescent Protein Knock-In Mice. *PLOS ONE,* 5**,** e13693-e13693.
621 Sato, E., Shick, H. E., Ransohoff, R. M. & Hirose, K. 2008. Repopulation of cochlear macrophages in murine
622 hematopoietic progenitor cell chimeras: The role of CX3CR1. *Journal of Comparative Neurology,* 506**,**
623 930-942.
624 Sautter, N. B., Shick, E. H., Ransohoff, R. M., Charo, I. F. & Hirose, K. 2006. CC chemokine receptor 2 is
625 protective against noise-induced hair cell death:: Studies in CX3CR1 mice. *Jaro-Journal of the*
626 *Association for Research in Otolaryngology,* 7**,** 361-372.
627 Shechter, R., Miller, O., Yovel, G., Rosenzweig, N., London, A., Ruckh, J., Kim, K. W., Klein, E., Kalchenko, V.,
628 Bendel, P., Lira, S. A., Jung, S. & Schwartz, M. 2013. Recruitment of Beneficial M2 Macrophages to
629 Injured Spinal Cord Is Orchestrated by Remote Brain Choroid Plexus. *Immunity,* 38**,** 555-569.
630 Shi, X. 2009. Cochlear pericyte responses to acoustic trauma and the involvement of hypoxia-inducible factor-
631 1α and vascular endothelial growth factor. *American Journal of Pathology,* 174**,** 1692-1704.
632 Shi, X. 2010. Resident macrophages in the cochlear blood-labyrinth barrier and their renewal via migration of
633 bone-marrow-derived cells. *Cell and Tissue Research,* 342**,** 21-30.

Shi, X. R. 2016. Pathophysiology of the cochlear intrastrial fluid-blood barrier (review). *Hearing Research,* 338**,** 52-63.
Shihan, M. H., Novo, S. G., Le Marchand, S. J., Wang, Y. & Duncan, M. K. 2021. A simple method for quantitating confocal fluorescent images. *Biochemistry and Biophysics Reports,* 25.
Shin, S. H., Jung, J. S., Park, H. R., Sim, N. S., Choi, J. Y. & Bae, S. H. 2022. The Time Course of Monocytes Infiltration After Acoustic Overstimulation. *Frontiers in Cellular Neuroscience,* 16.
Simard, A. R., Soulet, D., Gowing, G., Julien, J. P. & Rivest, S. 2006. Bone marrow-derived microglia play a critical role in restricting senile plaque formation in Alzheimer's disease. *Neuron,* 49**,** 489-502.
Stowell, R. D., Sipe, G. O., Dawes, R. P., Batchelor, H. N., Lordy, K. A., Whitelaw, B. S., Stoessel, M. B., Bidlack, J. M., Brown, E., Sur, M. & Majewska, A. K. 2019. Noradrenergic signaling in the wakeful state inhibits microglial surveillance and synaptic plasticity in the mouse visual cortex. *Nature Neuroscience,* 22**,** 1782-1792.
Sung, C. Y. W., Hayase, N., Yuen, P. S. T., Lee, J., Fernandez, K., Hu, X., Cheng, H., Star, R. A., Warchol, M. E. & Cunningham, L. L. 2024. Macrophage depletion protects against cisplatin-induced ototoxicity and nephrotoxicity. *Science Advances,* 10.
Tan, W. J. T., Thorne, P. R. & Vlajkovic, S. M. 2016. Characterisation of cochlear inflammation in mice following acute and chronic noise exposure. *Histochemistry and Cell Biology,* 146**,** 219-230.
Tornabene, S. V., Sato, K., Pham, L., Billings, P. & Keithley, E. M. 2006. Immune cell recruitment following acoustic trauma. *Hearing Research,* 222**,** 115-124.
Van Furth, R. & Cohn, Z. A. 1968. The origin and kinetics of mononuclear phagocytes. *The Journal of experimental medicine,* 128**,** 415-435.
Van Hove, H., Antunes, A. R. P., De Vlaminck, K., Scheyltjens, I., Van Ginderachter, J. A. & Movahedi, K. 2020. Identifying the variables that drive tamoxifen-independent CreERT2 recombination: Implications for microglial fate mapping and gene deletions. *European Journal of Immunology,* 50**,** 459-463.
Whitelaw, D. M. & Bell, M. 1966. The Intravascular Lifespan of Monocytes. *Blood,* 28**,** 455-464.
Xu, Y., Zhan, Y., Lew, A. M., Naik, S. H. & Kershaw, M. H. 2007. Differential Development of Murine Dendritic Cells by GM-CSF versus Flt3 Ligand Has Implications for Inflammation and Trafficking. *The Journal of Immunology,* 179**,** 7577-7584.
Yang, J., Zhang, L., Yu, C., Yang, X.-F. & Wang, H. 2014. Monocyte and macrophage differentiation: circulation inflammatory monocyte as biomarker for inflammatory diseases. *Biomarker Research,* 2**,** 1.
Yang, W., Vethanayagam, R. R., Dong, Y., Cai, Q. & Hu, B. H. 2015. Activation of the Antigen Presentation Function of Mononuclear Phagocyte Populations Associated with the Basilar Membrane of the Cochlea after Acoustic Overstimulation. *Neuroscience,* 303**,** 1-15.
Yang, Y., Dai, M., Wilson, T. M., Omelchenko, I., Klimek, J. E., Wilmarth, P. A., David, L. L., Nuttall, A. L., Gillespie, P. G. & Shi, X. 2011. Na+/K+-ATPase α1 Identified as an Abundant Protein in the Blood-Labyrinth Barrier That Plays an Essential Role in the Barrier Integrity. *PLOS ONE,* 6**,** e16547-e16547.
Yona, S., Kim, K. W., Wolf, Y., Mildner, A., Varol, D., Breker, M., Strauss-Ayali, D., Viukov, S., Guilliams, M., Misharin, A., Hume, D. A., Perlman, H., Malissen, B., Zelzer, E. & Jung, S. 2013. Fate mapping reveals origins and dynamics of monocytes and tissue macrophages under homeostasis. *Immunity,* 38**,** 79-91.
Zhang, F., Dai, M., Neng, L., Zhang, J. H., Zhi, Z., Fridberger, A. & Shi, X. 2013. Perivascular macrophage-like melanocyte responsiveness to acoustic trauma-a salient feature of strial barrier associated hearing loss. *FASEB Journal,* 27**,** 3730-3740.
Zhang, W., Dai, M., Fridberger, A., Hassan, A., Degagne, J., Neng, L., Zhang, F., He, W., Ren, T., Trune, D., Auer, M. & Shi, X. 2012. Perivascular-resident macrophage-like melanocytes in the inner ear are essential for the integrity of the intrastrial fluid-blood barrier. *Proceedings of the National Academy of Sciences of the United States of America,* 109**,** 10388-10393.
Zigmond, E., Varol, C., Farache, J., Elmaliah, E., Satpathy, A. T., Friedlander, G., Mack, M., Shpigel, N., Boneca, I. G., Murphy, K. M., Shakhar, G., Halpern, Z. & Jung, S. 2012. Ly6Chi Monocytes in the Inflamed Colon Give Rise to Proinflammatory Effector Cells and Migratory Antigen-Presenting Cells. *Immunity,* 37**,** 1076-1090.

686 **DECLARATIONS**

687 **Availability of data and materials:** All data are available in the main text or the supplementary materials.

688

689 **Acknowledgements:** We thank Dr. Astrid Cardona and her lab members at the University of Texas, San Antonio
690 (UTSA) for sharing the flow cytometry protocol for immunophenotyping of CX_3CR1 lineage in the blood of adult
691 mice.

692

693 **Funding:** Supported by a grant from R01 DC019918 (TK; National Institute on Deafness and Other
694 Communication Disorders).

695

696 **Author's contributions:** TK conceptualized and designed the study. SVM, ARS, LB, and TK ran experiments.
697 SVM, ARS, EP, and TK analyzed and interpreted data. TK and SVM co-wrote the manuscript.

698

699 **Ethics declarations:**

700 **Competing interests**: The authors declare no competing interests.

701

702 **Ethics approval and consent to participate:** All aspects of animal care, procedure, and treatment were
703 carried out according to the guidelines of the Animal Studies Committee of Creighton University, Omaha, NE,
704 and Rutgers University, Piscataway, NJ.

705

706

707

708

709

710

711

712

713 **FIGURES AND FIGURE LEGENDS**

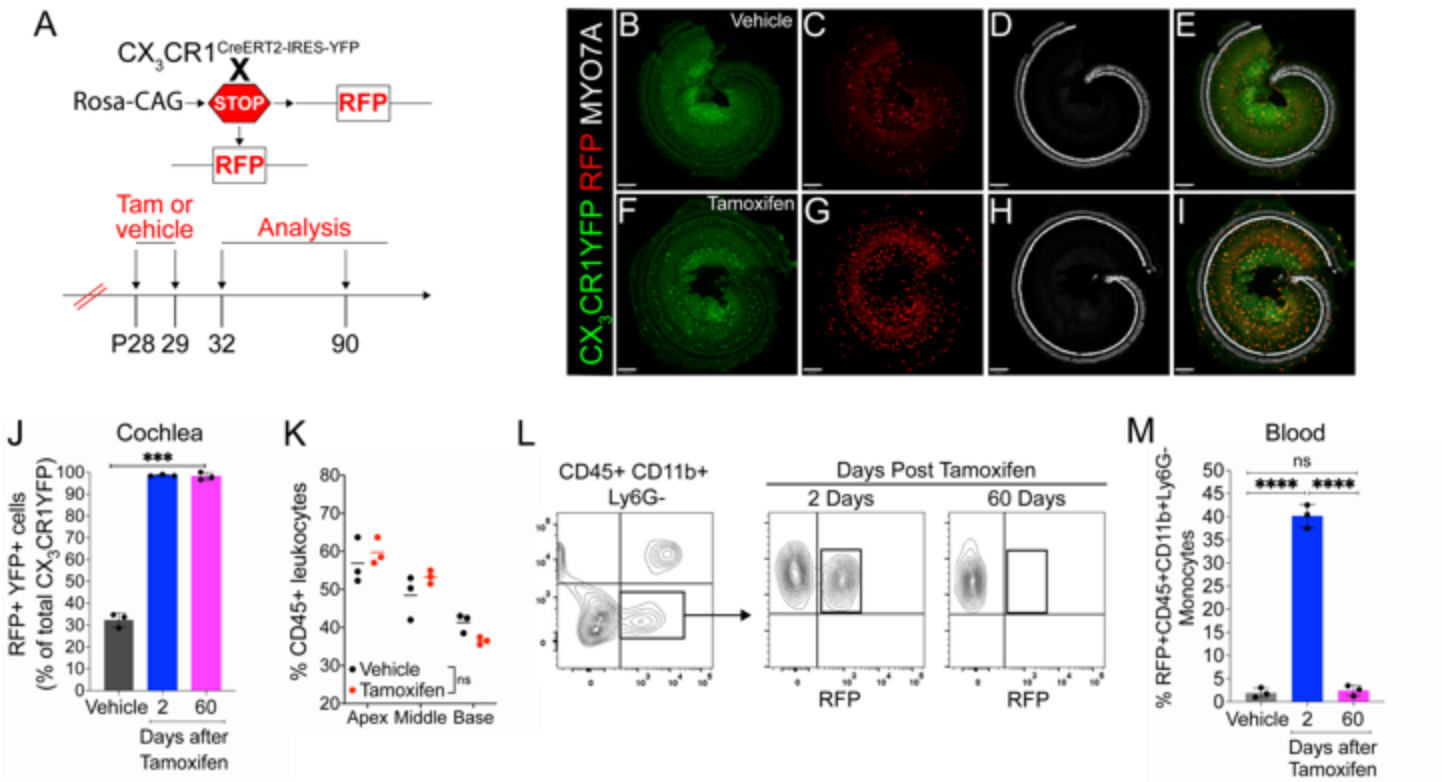

714 **Figure and figure legend 1. Cre recombination efficiency in CX_3CR1-lineage leukocytes in adult mouse**
715 **cochlea and blood in $CX_3CR1^{YFP-CreER/wt}$:$R26^{RFP}$ mice.** (A) Experimental regime. (B-I) Representative confocal
716 images of cochlear whole mounts immunostained to label for B, F, CX_3CR1-expressing macrophages (YFP/GFP,
717 green), C, G Cre recombination (RFP/tdTomato, red), D, H, sensory hair cells (Myosin 7A, white), and E, I,
718 merged (yellow) at 60 days post vehicle (corn oil) (B-E) or tamoxifen (F-I) injections. Scale bar = 130 µm. (J)
719 Percentage of Cre recombination (RFP+) in YFP+ CX_3CR1-expressing cochlear macrophages at 60 days after
720 vehicle injections or at 2 and 60 days after tamoxifen injections. (K) Percentage of CD45+ leukocytes in the
721 cochleae of vehicle- and tamoxifen-injected mice at 60 days post-injections. (L, M) Blood flow cytometry gating
722 strategy (L) and quantification (M) of CX_3CR1 lineage (CD45+, CD11b+, Ly6G-) (black box in L). N=3 mice per
723 condition in J, K, and M. Data in J, K, and M are presented as Mean±SD. ***$p<0.001$, ****$p<0.0001$, ns, not
724 significant; one-way ANOVA (J, M) or two-way ANOVA (K).

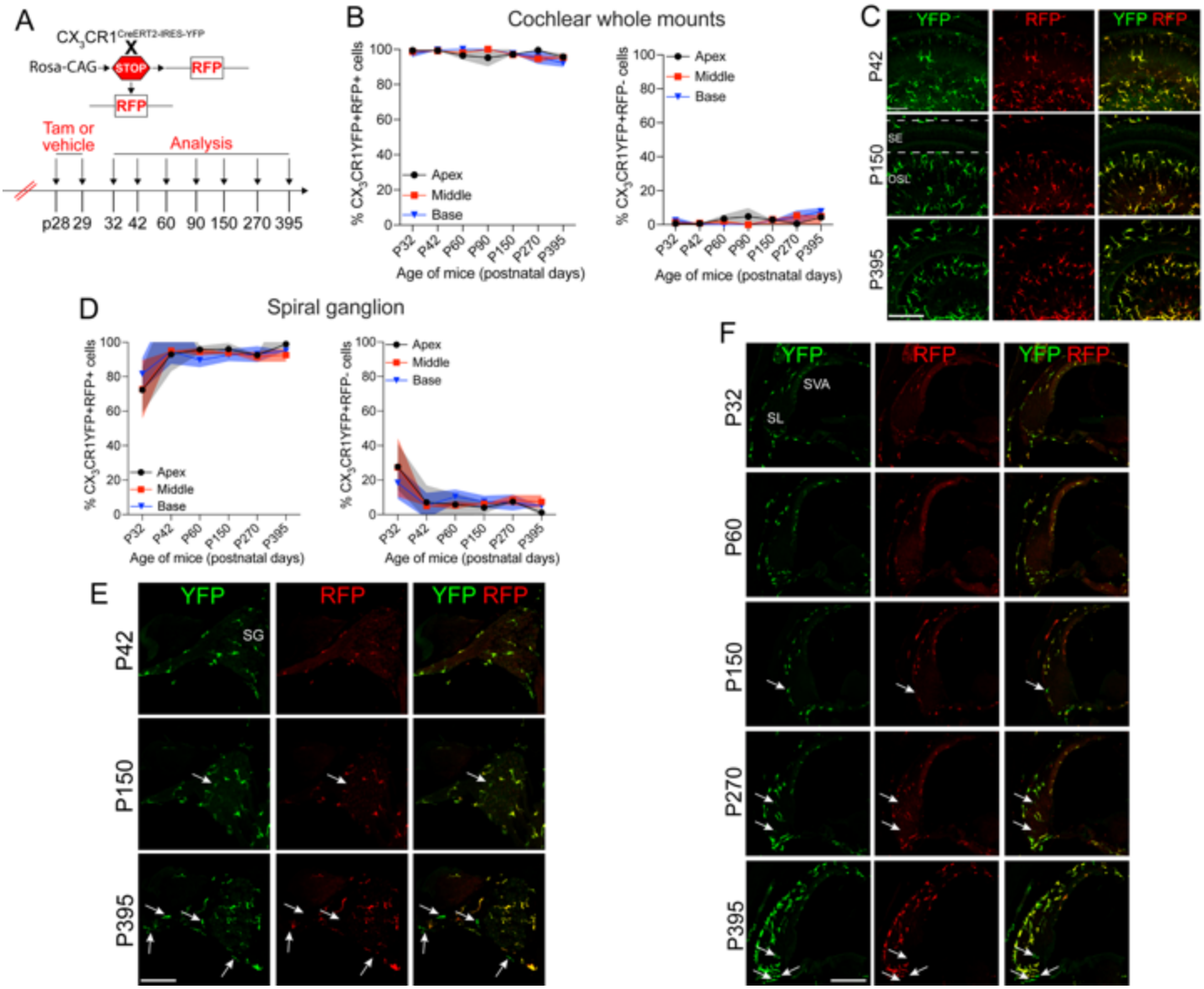

725

726 **Figure and figure legend 2. Slow turnover of cochlear resident macrophages in an adult mouse under**
727 **steady state.** (A) Experimental regime. (B) The percentage of $CX_3CR1YFP+$ RFP+ RM (left) and $CX_3CR1YFP+$
728 RFP- Mo/Mo-M (right) in mature cochlear whole mounts across a period of one year shows a slow turnover of
729 resident macrophages in steady state. (C) Representative micrographs of the middle region of the cochlea show
730 the presence of mostly the resident macrophages (YFP+ RFP+, yellow) at P42, P150, and P395. SE: sensory
731 epithelium, OSL: Osseous spiral lamina. (D) The percentage of $CX_3CR1YFP+$ RFP+ RM (left) and $CX_3CR1YFP+$
732 RFP- Mo/Mo-M (right) in the spiral ganglion (SG) across a period of one year shows a slow turnover of resident
733 macrophages in steady state. (E) Representative confocal micrographs of the spiral ganglion show the presence
734 of mostly resident macrophages (YFP+ RFP+, yellow) and very few monocyte-derived macrophages (YFP+

735 RFP-, green, white arrows). (F) Representative confocal micrographs showing spiral ligament (SL) and stria
736 vascularis (SVA) of the lateral wall of the basal cochlear turn show the presence of mostly resident macrophages
737 (YFP+ RFP+, yellow) and very few monocyte-derived macrophages (YFP+ RFP-, green, white arrows). N=3
738 mice per time point in B and D. Data in B and D are presented as Mean±SD. Scale bar = 50 μm in all panels of
739 C, E, and F. White arrows in E and F show the presence of YFP+ RFP- recruited macrophages (Mo/Mo-M) in
740 the spiral ganglion and lower spiral ligament, respectively, as a function of biological aging.
741
742
743
744
745
746
747
748
749
750
751
752
753
754
755
756
757
758
759
760
761

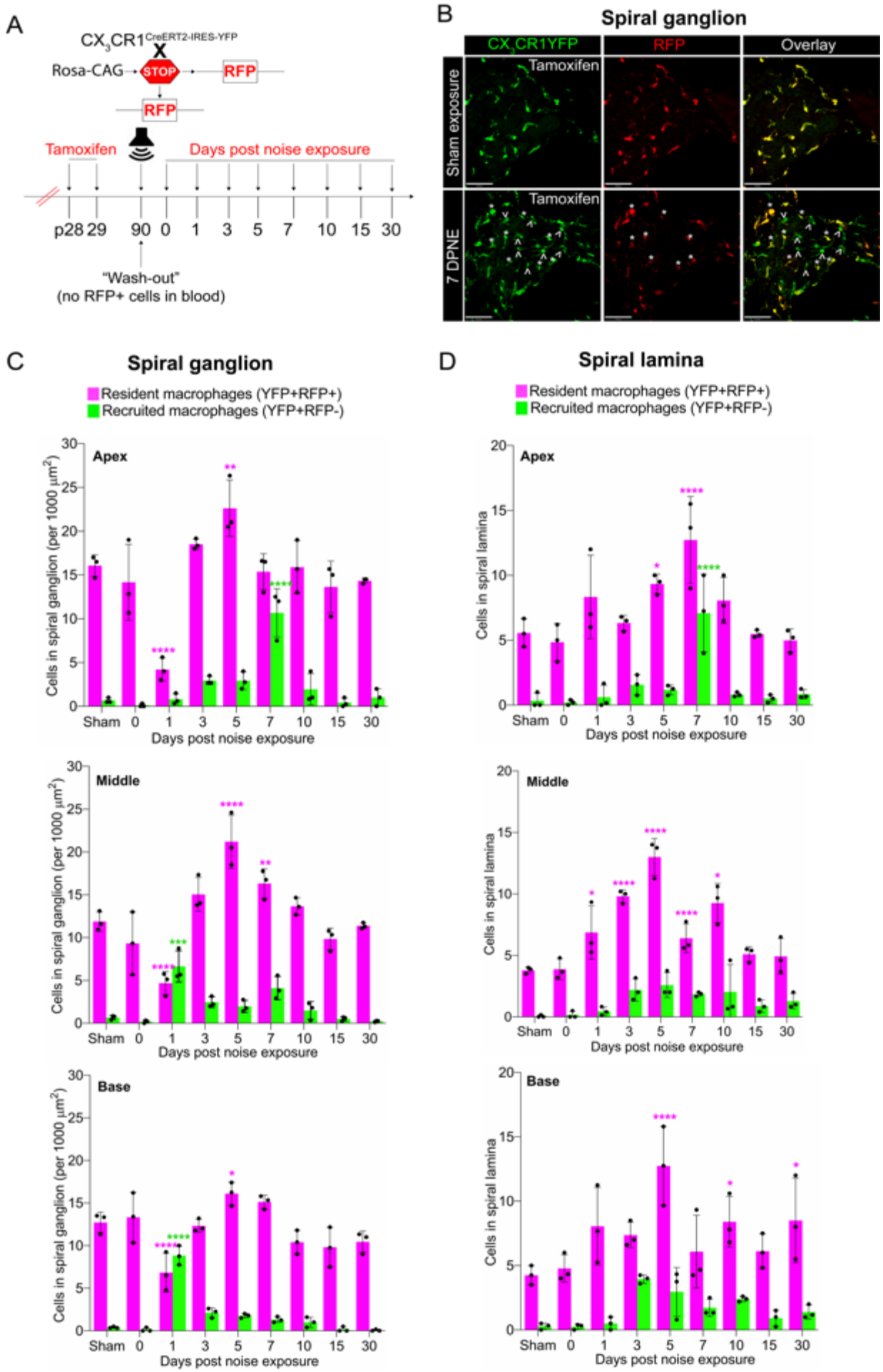
A
CX3CR1CreERT2-IRES-YFP
X
Rosa-CAG
STOP
RFP
RFP
Tamoxifen
Days post noise exposure
p28 29 90 0 1 3 5 7 10 15 30
"Wash-out"
(no RFP+ cells in blood)
B
Spiral ganglion
CX3CR1YFP
RFP
Overlay
Sham exposure
7 DPNE
Tamoxifen
Tamoxifen
C
Spiral ganglion
Resident macrophages (YFP+RFP+)
Recruited macrophages (YFP+RFP-)
Apex
Middle
Base
Cells in spiral ganglion (per 1000 µm2)
Sham 0 1 3 5 7 10 15 30
Days post noise exposure
D
Spiral lamina
Resident macrophages (YFP+RFP+)
Recruited macrophages (YFP+RFP-)
Apex
Middle
Base
Cells in spiral lamina
Sham 0 1 3 5 7 10 15 30
Days post noise exposure

788 **Figure and figure legend 3. Fate mapping with $CX_3CR1^{YFP-CreER/wt}$:$R26^{RFP}$ mice distinguishes CX_3CR1-**
789 **expressing RM and Mo/Mo-M in the neuronal region of the cochlea after acoustic trauma.** (A) Experimental
790 regime. (B) Representative confocal images of the spiral ganglion from tamoxifen-injected Cre mice after sham-
791 exposure (top) and at 7 days after acoustic trauma (bottom) shows the presence of only resident macrophages
792 (yellow overlay) after sham exposure and resident macrophages (YFP+ RFP+, yellow overlay, white asterisks)
793 and recruited monocyte-derived macrophages (YFP+ RFP-, green overlay, white arrows) after acoustic trauma.
794 Scale bar = 50 μm (C, D) Quantification of resident and recruited macrophages in the apical, middle, and basal
795 spiral ganglion (C) and osseous spiral lamina (D) on different days after exposure. Data in C and D are presented
796 as Mean±SD from N=3 mice per time point. *$p<0.05$, ** $p< 0.01$, ***$p<0.001$, ****$p<0.0001$; one-way ANOVA
797 comparing macrophage numbers at different days post noise exposure with the sham group. Asterisks are color-
798 coded based on resident (magenta) or recruited (green) macrophages, as shown in the graph legends.
799
800
801
802
803
804
805
806
807
808
809
810
811
812
813
814

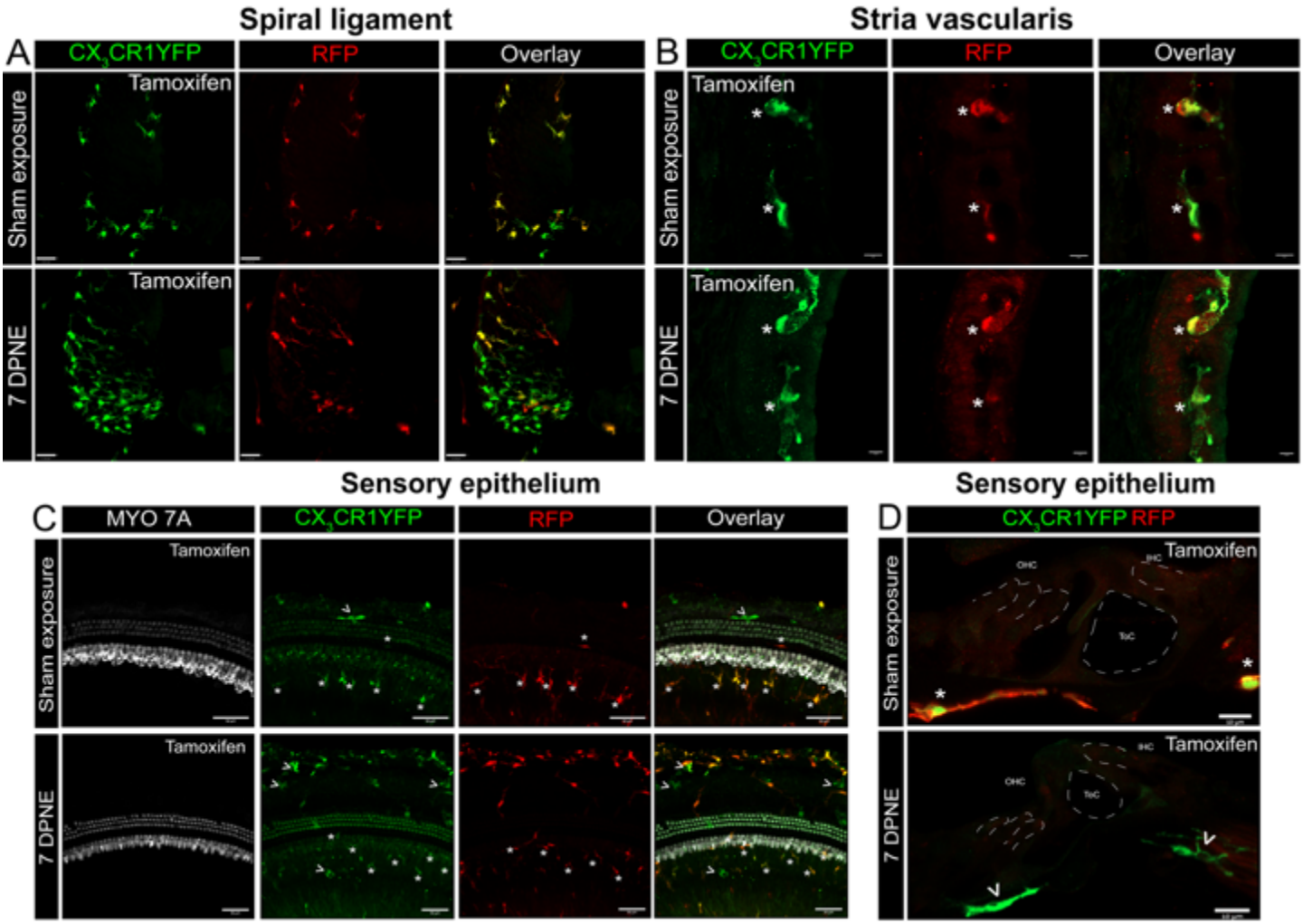

Figure and figure legend 4. CX_3CR1-expressing RM and Mo/Mo-M in the spiral ligament, stria vascularis, and sensory epithelium of the cochlea after acoustic trauma. Representative confocal images of the spiral ligament (A), stria vascularis (B), and sensory epithelium (C, D) from tamoxifen-injected Cre mice after sham-exposure (top) and at 7 days after acoustic trauma (bottom). White asterisks show YFP+ RFP+ resident macrophages (yellow overlay), and white arrows show YFP+ RFP- recruited monocyte/monocyte-derived macrophages (green overlay). Mo/Mo-M (green) are present in the lower spiral ligament as the primary site for macrophage accumulation (A), around the sensory epithelium (D), but not in the stria vascularis (B) of the noise-injured cochlea. Scale bars = 30 μm (A), 5 μm (B), 50 μm (C), and 10 μm (D).

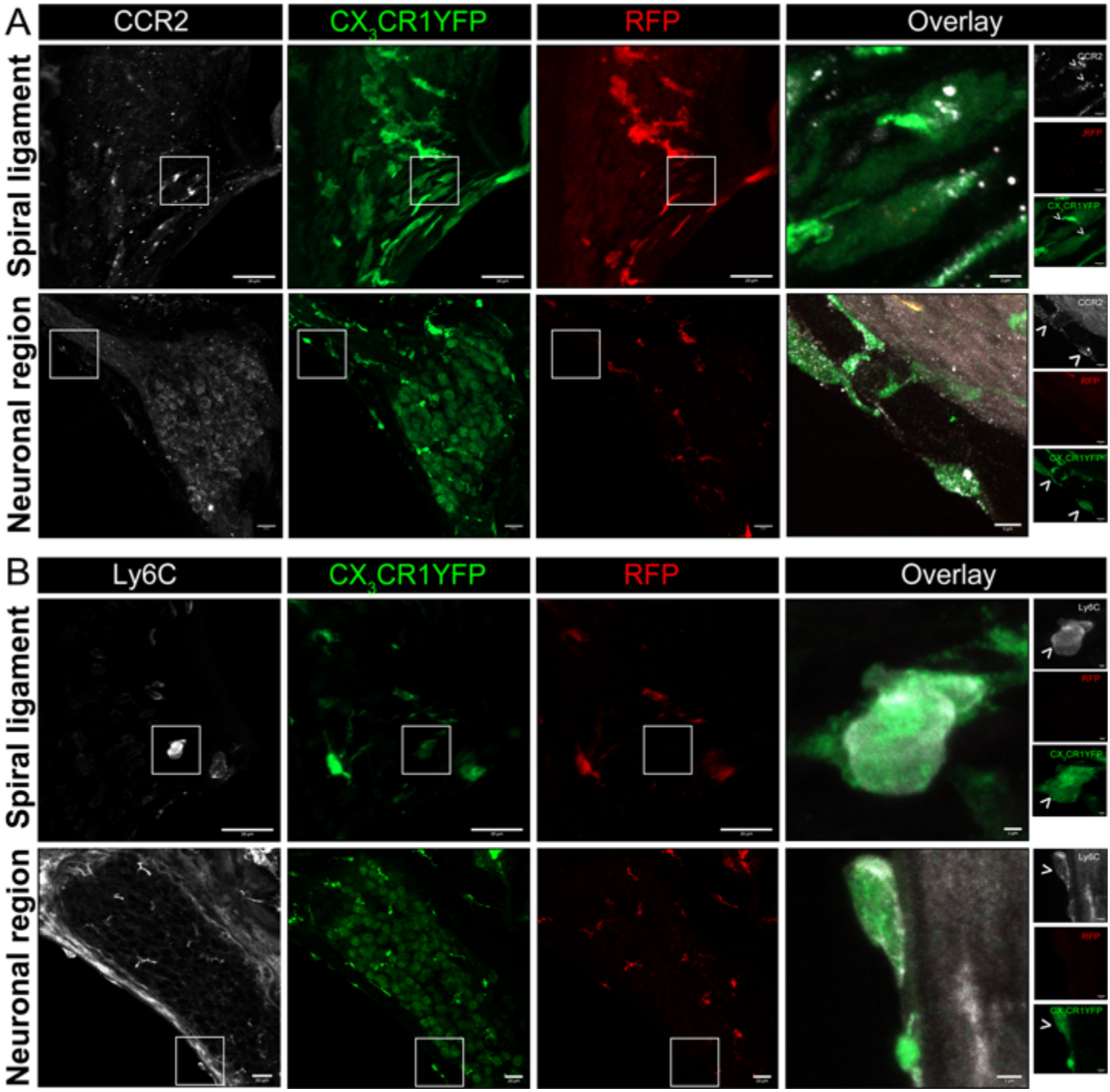

828

829 **Figure and figure legend 5. Blood-circulating recruited Mo/Mo-M express classical monocyte markers,**
830 **CCR2 and LY6C, in the noise-injured cochlea.** Representative confocal images showing expression of (A)
831 CCR2 and (B) Ly6C in the blood-circulating recruited Mo/Mo-M (YFP+ RFP-) in the lower spiral ligament and
832 neuronal region (Rosenthal's canal and spiral lamina) after 3 days of exposure to 112 dB SPL noise level for 2
833 hours. Insets (white boxes) show the higher magnification of CCR2- and Ly6C-expressing recruited Mo/Mo-M in

834 the overlay images. Note: Ly6C is also expressed in the RM (YFP+ RFP+) in the spiral ganglion at 3 DPNE (B),
835 which could be associated with an inflammatory response/phenotype at the early stages of cochlear injury.
836
837
838
839
840
841
842
843
844
845
846
847
848
849
850
851
852
853
854
855
856
857
858
859
860

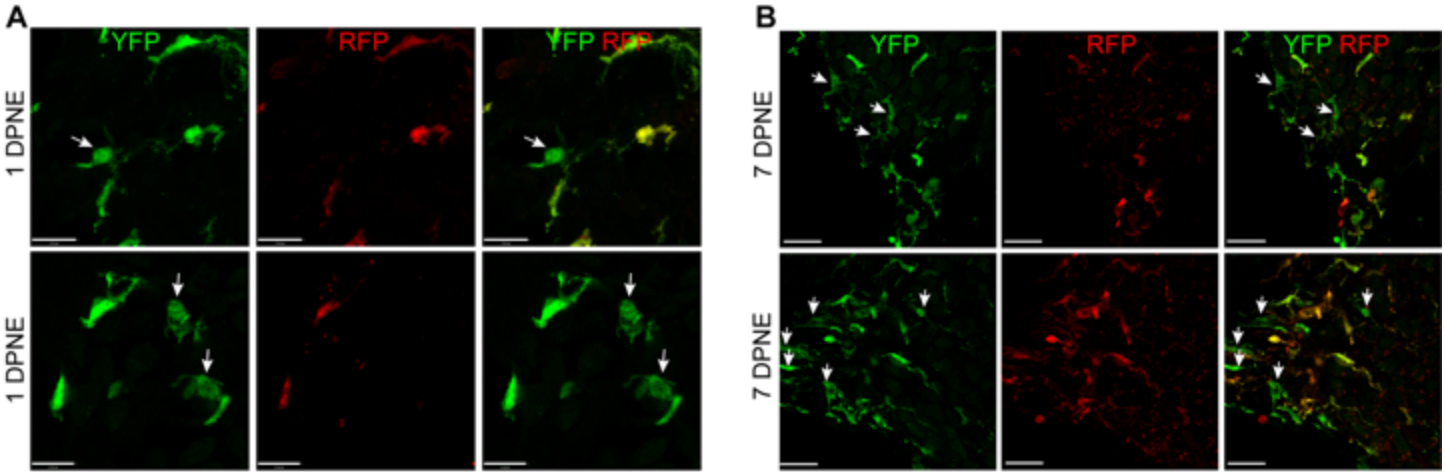

Figure and figure legend 6. Morphology of CX_3CR1-expressisng RM and Mo/Mo-M. Representative confocal micrographs showing indistinguishable morphology of CX_3CR1-expressing resident (YFP+ RFP+) and recruited (YFP+ RFP-, white arrows) macrophages in the spiral ganglion at 1 (A) and 7 (B) days post-noise exposure. Note: The recruited circulating Mo was transformed from being round or less ramified at 1 DPNE to more ramified by 7 DPNE (white arrows). This suggests that the infiltrated circulating Mo may differentiate into cochlear RM. Scale bars = 17 μm (top panel), 13 μm (bottom panel) in A and 20 μm in B, respectively.

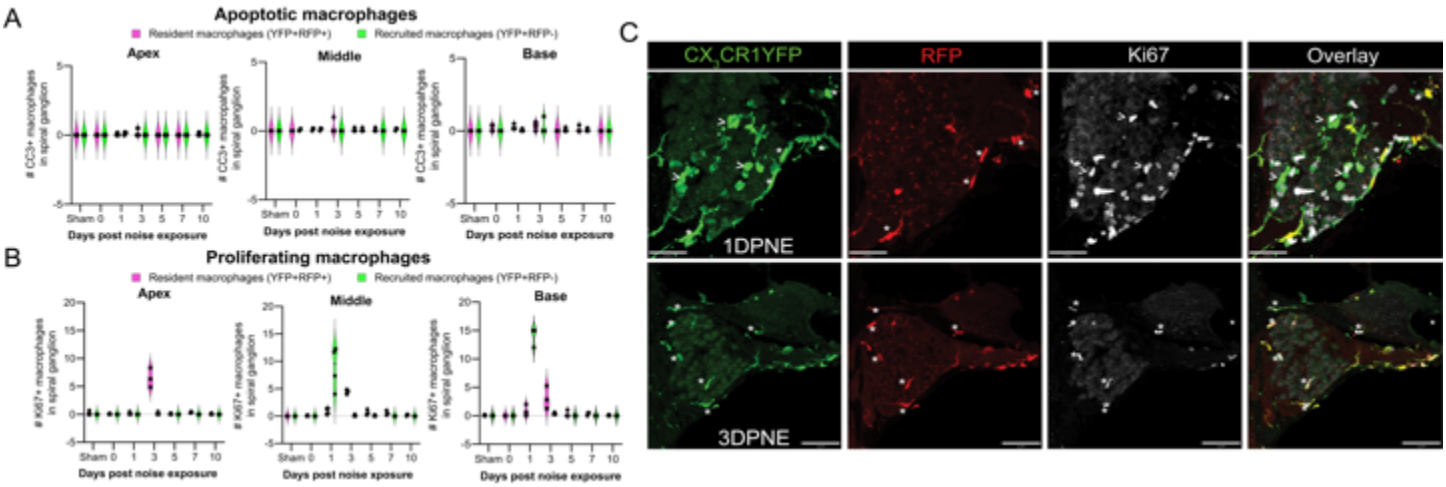

Figure and figure legend 7. Fate of CX_3CR1-expressisng RM and Mo/Mo-M. Number of (A) Cleaved caspase 3 (CC3) and (B) Ki67 positive macrophages in the apical, middle, and basal spiral ganglion on different days after noise exposure. Data is plotted as Mean±SD. N=3-4 mice per recovery time. (C) Representative confocal micrographs showing Ki67 positive resident (YFP+ RFP+, white asterisks) and recruited (YFP+ RFP-, white arrows) macrophages in the spiral ganglion of the middle turn at 1- and 3-days post noise exposure. Scale bar = 31 µm (top panel) and 70 µm (bottom panel) in C.

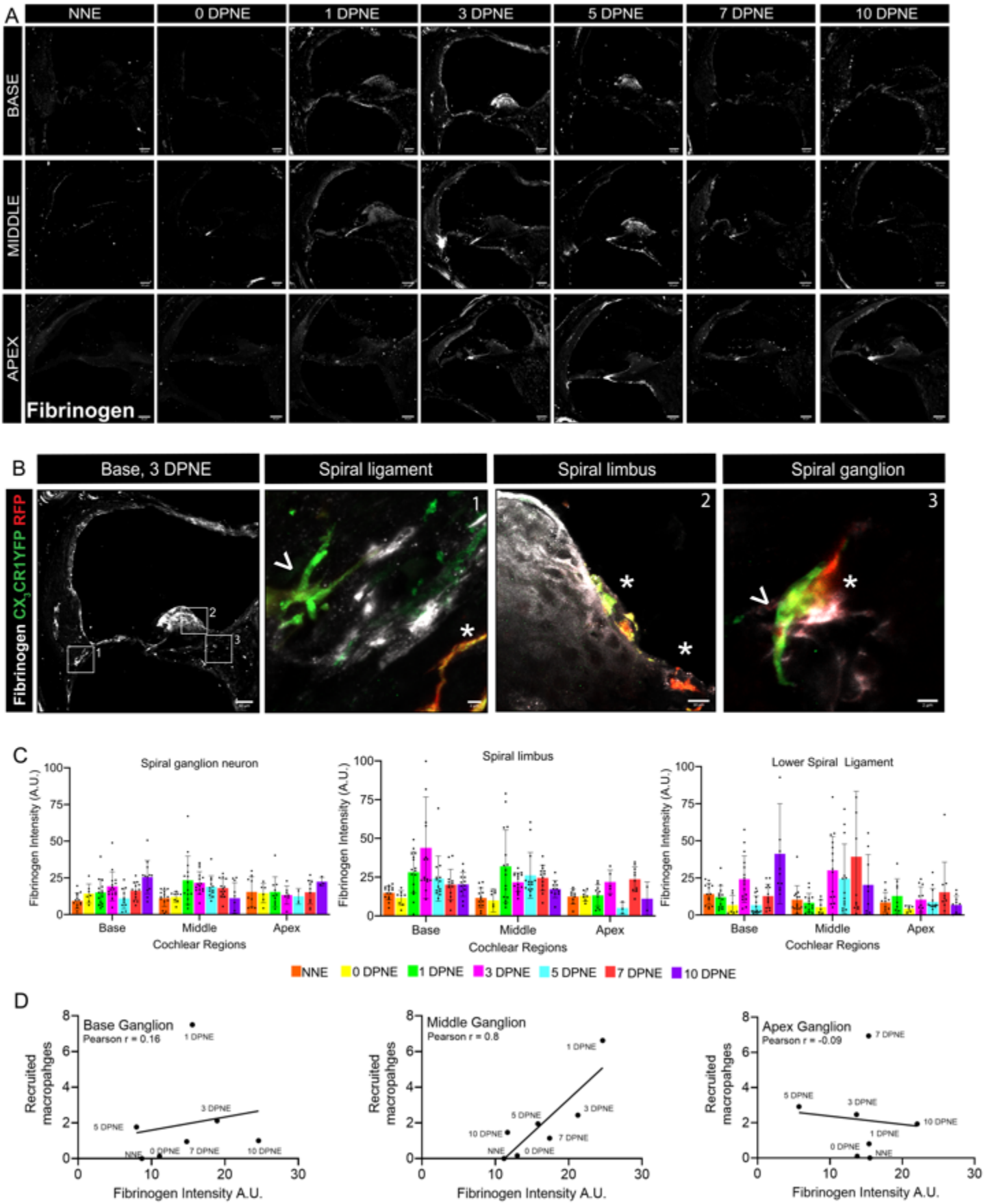
A
NNE
0 DPNE
1 DPNE
3 DPNE
5 DPNE
7 DPNE
10 DPNE
BASE
MIDDLE
APEX
Fibrinogen
B
Base, 3 DPNE
Spiral ligament
Spiral limbus
Spiral ganglion
Fibrinogen CX3CR1YFP RFP
C
Spiral ganglion neuron
Spiral limbus
Lower Spiral Ligament
Fibrinogen Intensity (A.U.)
Base
Middle
Apex
Cochlear Regions
NNE
0 DPNE
1 DPNE
3 DPNE
5 DPNE
7 DPNE
10 DPNE
D
Base Ganglion
Pearson r = 0.16
Middle Ganglion
Pearson r = 0.8
Apex Ganglion
Pearson r = -0.09
Recruited macropahges
Fibrinogen Intensity A.U.

902

903 **Figure and figure legend 8. Fibrinogen extravasation from blood and deposition in the cochlear labyrinth**
904 **indicates vascular aberration and positively correlates with the recruitment of Mo/Mo-M after acoustic**
905 **trauma.** (A) Representative confocal images of fibrinogen extravasation in the base, middle, and apex cochlear
906 turns at different time points after an acoustic trauma of 112 dB SPL for 2 hours at 8-16 kHz octave band. Scale
907 bar = 50 μm. (B) Representative high magnification confocal images showing fibrinogen fluorescence and
908 juxtaposed RM (white asterisk) and Mo/Mo-M (white arrow) in the lower spiral ligament (1), spiral limbus (2), and
909 spiral ganglion (3) at 3 DPNE. (C) Fibrinogen fluorescent intensity in arbitrary units (A.U.) in apex, middle, and
910 base spiral ganglion, lower spiral ligament, and spiral lamina as a function of days post noise exposure (DPNE).
911 Data is plotted as Mean±SD. Each dot in the graphs in C represents cochlear cross sections from 2 to 4 animals
912 per time point. (D) Pearson's correlation analysis between fibrinogen intensity and recruited Mo/Mo-M density in
913 the base, middle, and apex spiral ganglia at different time points after an acoustic trauma. r, Pearson correlation
914 coefficient.
915
916
917
918
919
920
921
922
923
924
925

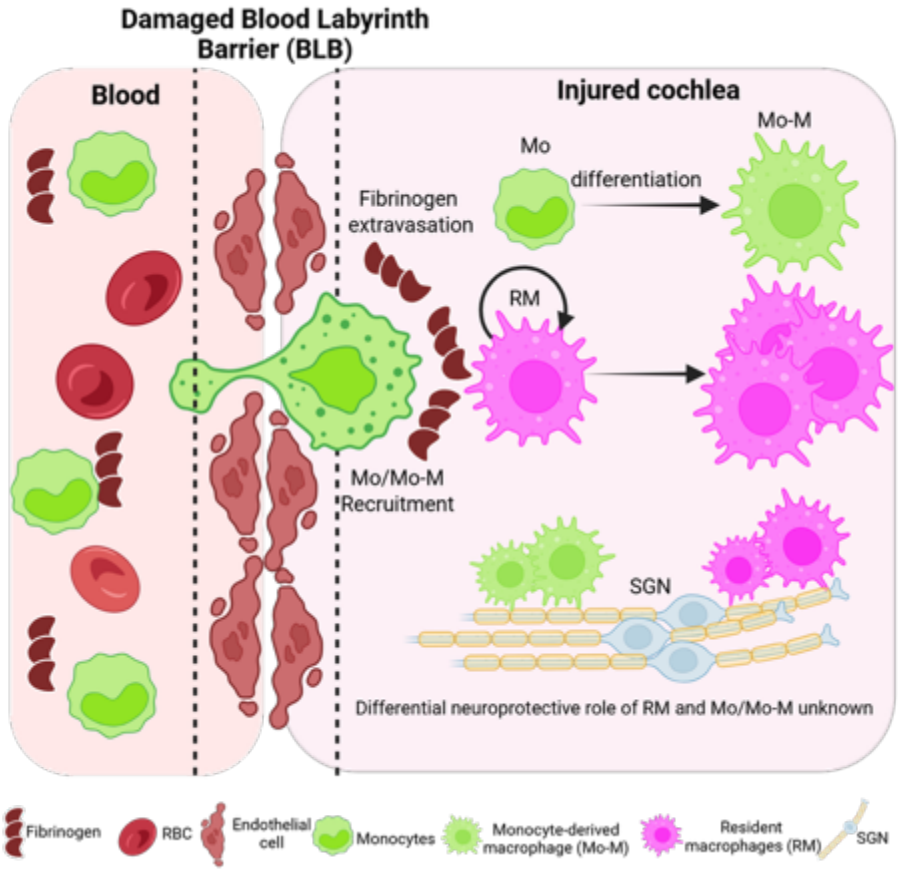

Figure and figure legend 9. Working model of the ontogeny and dynamics of resident and recruited macrophages in the injured cochlea. Schematic illustrating disruption of the blood-labyrinth barrier (BLB), fibrinogen glycoprotein extravasation from blood, and subsequent recruitment of circulating monocytes (green) into the injured cochlea following an acute (2 hours) acoustic trauma imparting permanent hearing loss. The short-lived recruited monocytes may ultimately differentiate into macrophages (monocyte-derived macrophages, Mo-M). The long-lived cochlear resident macrophages (RM, magenta) undergo self-renewal and expansion in the injured cochlea. The overall increase in the number of macrophages in the acute noise-injured cochlea is attributed to the recruitment of blood-circulating monocytes, their prospective differentiation into macrophages, and the *in-situ* proliferation of resident (local) macrophages. Defining the dynamics and the differential neuroprotective functions of CX_3CR1-expressing cochlear resident and recruited macrophages in acute and chronic pathological cochleae is under investigation. The illustration is created in BioRender.

950 **TABLE AND TABLE LEGENDS**

951 **Table 1.** List of primers to genotype mice by PCR.

Mouse Strain	Primers		Mouse ID (Jax stock number)	RRID #
Cre (generic)	Forward	5'-GCATTACCGGTCGATGCAACGAGTGATGAG-3'	021160	IMSR_JAX:021160
	Reverse	5'-GAGTGAACGAACCTGGTCGAAATCAGTGCG-3'		
tdTomato	Forward	5'-GGCATTAAAGCAGCGTATCC-3'	007914	IMSR_JAX:007914
	Reverse	5'-CTGTTCCTGTACGGCATGG-3'		

952

953 **Table 2.** List of antibodies and probes.

Probes and antibodies	Host species	Isotype	Clone	Dilution/ volume	Vendor	Catalog #	RRID #
Anti-Mouse CD16/CD32 (Fc block)	Rat	IgG2bκ	2.4G2	2 µL/ 100 µL of cell suspension	BD Biosciences	553142	AB_394657
Live/Dead Stain	NA	NA	NA	1µL of 1:100 dilution	Invitrogen	L34967	NA
APC-CD45	Rat	IgG2bκ	30-F11	1:5	BD Biosciences	559864	AB_398672
BV711-CD11b	Rat	IgG2b	M1/70	1:5	BioLegend	101241	AB_11218791
PECy7-Ly6G	Rat	IgG2b	RB6-8C5	1:2	Thermo Fisher Scientific	25-5931-81	AB_469662
APC-CCR2	Rat	IgG2b	475301	1:100	R&D Systems	FAB5538A	AB_10645617
anti-CD45	Goat	IgG	NA	1:50	R&D Systems	AF114	AB_442146
anti-GFP/YFP	Rabbit	IgG	NA	1:500	Thermo Fisher Scientific	A-11122	AB_221569
anti-GFP/YFP	Chicken		NA	1:500	Aves lab	GFP-1010	AB_2307313
anti-Cleaved Caspase 3	Rabbit	IgG	NA	1:400	Cell Signaling	9661S	AB_2341188
anti-Ki67	Rabbit	IgG	NA	1:200	Abcam	ab15580	AB_443209
anti-Fibrinogen	Rabbit	IgG	NA	1:500	Dako, Agilent	A0080	AB_2894406
anti-Ly6C	Mouse	IgG1	NA	1:100	Santa Cruz Biotechnology	sc-271811	AB_10707825
anti-CCR2	Rabbit	IgG	NA	1:100	Abcam	ab216863	AB_2832204

954 (NA – not applicable)